

1 GEAR1: a Global Earthquake Activity Rate model constructed from
2 geodetic strain rates and smoothed seismicity

3 P. Bird¹, D. D. Jackson¹, Y. Y. Kagan¹, C. Kreemer², and R. S. Stein³

4 ¹Department of Earth, Planetary, and Space Sciences, University of California-Los Angeles

5 ²Nevada Bureau of Mines and Geology, and Seismological Laboratory, University of Nevada-
6 Reno

7 ³U.S. Geological Survey, Menlo Park, California

8 Final manuscript of 3 July 2015, accepted by **BSSA**

9 This submission includes Electronic Supplement files, including additional text and references
10 on scoring of forecasts, tables of scoring results, and source code and data files needed
11 to reproduce our forecast.

12 ABSTRACT

13 GEAR1 estimates the rate of shallow earthquakes with magnitudes 6 through 9 everywhere on
14 Earth. It was designed to be reproducible and testable. Our preferred hybrid forecast is a log-
15 linear blend of two parent forecasts based on the Global CMT catalog (smoothing 4602 $m \geq$
16 5.767 shallow earthquakes, 1977-2004) and the Global Strain Rate Map version 2.1 (smoothing
17 22415 GPS velocities), optimized to best forecast the 2005-2012 GCMT catalog. Strain rate is a
18 proxy for fault stress accumulation, and earthquakes indicate stress release, so a multiplicative
19 blend is desirable, capturing the strengths of both approaches. This preferred hybrid forecast

20 outperforms its seismicity and strain rate parents; the chance that this improvement stems
21 from random seismicity fluctuations is less than 1%. The preferred hybrid is also tested against
22 the independent parts of the ISC-GEM catalog ($m \geq 6.8$ during 1918-1976) with similar success.
23 GEAR1 is an update of this preferred hybrid. Comparing GEAR1 to the Uniform California
24 Earthquake Rupture Forecast version 3 (UCERF3), net earthquake rates agree within 4% at $m \geq$
25 5.8 and at $m \geq 7.0$. The spatial distribution of UCERF3 epicentroids most resembles GEAR1 after
26 UCERF3 is smoothed with a 30-km kernel. As UCERF3 has been constructed to derive useful
27 information from fault geometry, slip rates, paleoseismic data, and enhanced seismic catalogs
28 (not used in our model), this is encouraging. To build parametric catastrophe bonds from
29 GEAR1, one could calculate the magnitude for which there is a 1% (or any) annual probability of
30 occurrence in local regions.

31 INTRODUCTION

32 Forecasting of seismicity is one of the more important practical applications of geophysical
33 research. Given a good forecast, societies have an opportunity to optimize their investments in
34 safer buildings and more resilient infrastructure; they also have a context in which to consider
35 offers and purchases of insurance. Objective scoring of forecasts can advance science by
36 testing hypotheses about earthquake generation and interaction (*e.g.*, Kelleher *et al.*, 1973;
37 McCann *et al.*, 1979; Kagan and Jackson, 1991; Nishenko and Sykes, 1993; Jackson and Kagan,
38 1993). Our objective in this paper is to build a testable global reference model of the expected
39 long-term rates of shallow earthquakes (those with hypocentroids no more than 70 km below
40 sea level) as a function of space and magnitude.

41 Only seismic catalogs, global plate boundary models, and Global Positioning System (GPS)
42 geodetic velocities provide uniform global coverage. Despite the obvious importance of
43 databases of active faults in seismic hazard studies, a comprehensive global inventory of active
44 faults does not yet exist. Few faults are well-mapped and fewer still have reliable slip rates,
45 geometries, and rakes needed to transform those faults into earthquake sources. Thus, the only
46 faults represented in this model are the principal plate boundaries such as subduction zones
47 and oceanic transforms, and even these are designated only as belts of straining, not as specific
48 planes. Also, only a global model that forecasts moderate-magnitude earthquakes implies a
49 sufficient rate of shocks to meet the testing requirement. We will demonstrate below that
50 competing global forecasts can be reliably ranked after only 1 to 8 years of testing, provided
51 that those forecasts have magnitude thresholds of approximately 5.8 to 7.0, respectively.

52 Previous forecasts have been constructed in two fundamentally different ways: by smoothing
53 of past catalog seismicity, or by applying seismic-coupling coefficients to faults with estimated
54 slip rates and other zones whose tectonic deformation rates have been measured. The creation
55 of a smoothed-seismicity forecast from a seismic catalog is straightforward, though it requires
56 careful research into optimization of the smoothing algorithm. A strength of smoothed-
57 seismicity methods is that they can capture hazards far from plate boundaries such as igneous
58 intrusions and gravity tectonics, such as the earthquakes of magnitude up to 7.4 which have
59 occurred in Hawaii. But a weakness is that existing catalogs are too short to include seismicity
60 along all plate boundaries and fault zones. Another issue is that if small earthquakes are used to
61 increase the sample size, induced earthquakes can be included as sources; it is not yet known
62 whether a better forecast of large earthquakes would be obtained by including, or omitting,

63 this induced seismicity. A further complication is that induced seismicity typically has a
64 different time-dependence than natural seismicity.

65 Tectonic forecasts require a reasonably complete database of deforming zones (*i.e.*, active
66 faults with their slip rates, and/or deforming areas with their strain-rates, and/or adjacent
67 plates and their Euler vectors). They also require a seismic catalog to calibrate the coupling
68 coefficients that will be used to convert fault slip rates and/or distributed strain rates to long-
69 term seismicity. However, if these sources can be grouped into a few tectonic zones of global
70 extent, then earthquakes accumulate rapidly in each zone, and it may be that only a few
71 decades of seismic catalog will suffice for calibration of a model with a modest number of
72 degrees of freedom. One weakness of tectonic forecasts is their potential to overestimate
73 seismicity of regions where faults creep aseismically. This is particularly important in
74 subduction zones, where some seismologists and geodesists believe that there is broad
75 diversity in the extent to which they are seismically coupled, while others (*e.g.*, McCaffrey,
76 2008) question whether this is measurable with present datasets.

77 One recent development in tectonic forecasting is the incorporation of relative plate rotations
78 and GPS-derived interseismic velocities. Such velocity-based tectonic models (*e.g.*, Bird, 2009;
79 Field *et al.*, 2013) impose kinematic compatibility on their faults and zones of straining,
80 reducing the risk that incomplete information about one fault, or one benchmark, will result in
81 incorrect seismicity forecasts.

82 Some forecasts and hazard models use a spatial composite approach, in which the well-known
83 faults are explicitly represented by traces, dips, and slip rates; but other deformation is

84 approximated by distributed sources derived from smoothed seismicity. The recent Uniform
85 California Earthquake Rupture Forecast version 3 (UCERF3) by Field *et al.* (2013) is such a
86 forecast.

87 Several groups have begun to pursue “hybrid,” “mixture,” or “ensemble” approaches, in which
88 two or more forecasts are combined to forecast the earthquake rate in every spatial cell (rather
89 than partitioning space as in a spatial-composite forecast). Rhoades and Gerstenberger (2009)
90 proposed a linear combination of two time-dependent models. Bird *et al.* (2010b) gave a
91 preview of global linear and log-linear hybrids of smoothed-seismicity and tectonic
92 components, with encouraging retrospective test results. Marzocchi *et al.* (2012) proposed a
93 Bayesian method for creating a linear-combination ensemble of existing forecasts with
94 optimized weights, and applied it to 6 existing Regional Earthquake Likelihood Models (RELMs)
95 for the southern California region (Field, 2007; Schorlemmer *et al.*, 2010). Rhoades *et al.* (2013,
96 2014) combined these same RELMs into many multiplicative hybrid models, and found a
97 greater improvement with multiplicative mixing than with linear combinations; prospective
98 testing of these hybrids is planned at the Collaboratory for the Study of Earthquake
99 Predictability (CSEP). Taroni *et al.* (2013) discuss four methods for linearly combining global
100 forecasts, and some reservations concerning available tests.

101 In this project we combine only two “parent” forecasts into a variety of hybrid forecasts. The
102 smoothed-seismicity parent forecast (or “Seismicity” for brevity) is a global forecast, on a $0.1^\circ \times$
103 0.1° grid, of shallow earthquakes with scalar moment $M > 10^{17.7}$ N m, based on GCMT shallow
104 seismicity (Ekstrom *et al.*, 2012, and references therein) during 1977-2004, computed by the
105 methods of Kagan and Jackson (1994, 2000, 2011). Basically, each epicentroid point (whose

106 magnitude is above the threshold) is convolved with a previously-optimized generic smoothing
107 kernel, and the results are summed to produce a map of forecast shallow earthquake rates
108 (above the same threshold). Each smoothing kernel is a product of functions of radius, source
109 earthquake magnitude, and azimuth. As a function of radius, the smoothing kernel is that of
110 equation (3) in Kagan and Jackson (2011), with parameter $r_s = 6$ km. The overall amplitude of
111 each smoothing kernel is a linear function of source earthquake magnitude, so larger events are
112 considered to forecast greater future seismicity. Also, since each GCMT centroid includes two
113 possible fault planes, each smoothing kernel is anisotropic, with greater future seismicity
114 forecast along the inferred strikes of the possible faults. There is no time-dependence in this
115 long-term forecast, and all earthquakes in the source catalog (including possible aftershocks)
116 are equally important, regardless of their sequence. A minimum or background level of
117 intraplate seismicity, integrating to 1% of total shallow seismicity, is uniformly distributed. This
118 Seismicity parent forecast is shown in **Figure 1A**.

119 Our second parent forecast is a tectonic forecast (or “Tectonics” for short) based on version 2.1
120 of the Global Strain Rate Map (GSRM2.1) of Kreemer *et al.* (2014). This strain-rate map was
121 based on plate-tectonic concepts and 22415 interseismic Global Positioning System (GPS)
122 velocities. Thus, it can be the basis for a self-consistent velocity-based forecast. It was
123 converted by Bird and Kreemer (2015) to a long-term tectonic forecast of seismicity using the
124 Seismic Hazard Inferred From Tectonics (SHIFT) hypotheses presented by Bird and Liu (2007).
125 The specific algorithm is very similar to that which Bird *et al.* (2010a) used to create an earlier
126 global tectonic forecast from GSRM (version 1). Basically, each strain-rate tensor is converted
127 to a long-term seismic moment rate by multiplication with the elastic shear modulus, the grid-

128 cell area, a dimensionless geometric factor, and a depth parameter called the coupled
129 seismogenic thickness. This coupled thickness value is taken from the “most comparable class”
130 of plate boundary in previous published compilations. Then, the seismic moment rate is
131 converted to earthquake rates by taking the normalized frequency/magnitude distribution of
132 the same “most comparable class” of plate boundary as a model. The algorithmic innovations
133 of Bird and Kreemer (2015) are that: (1) spatial smoothing was applied to the activity (both
134 strain-rate and seismicity) of offshore plate boundaries, and (2) velocity-dependence of seismic
135 coupling in subduction zones and continental convergent boundaries (Bird *et al.*, 2009) was
136 included. This forecast (**Figure 1B**) was originally created on a global grid of $0.25^\circ \times 0.20^\circ$ cells,
137 but has been resampled on a $0.1^\circ \times 0.1^\circ$ grid for this project. Numerical smoothing due to
138 resampling was minimal because 80% of the values transfer unchanged (when expressed as
139 epicentroid rate densities in $\text{m}^{-2} \text{s}^{-1}$), and the other 20% are simple equally-weighted averages
140 of the values in two adjacent cells within one row.

141 Both our two parent forecasts (discussed above) and our hybrid forecasts (discussed below)
142 share a common feature: They are forecasts of total seismicity, with no use of declustering and
143 no distinction between “mainshocks” and “aftershocks.” This feature is motivated by the lack
144 of *in-situ* physical distinctions between these two classes, by the lack of community agreement
145 on an optimal declustering scheme, and by consideration of likely misclassifications that would
146 result from catalog boundaries in space, time, and magnitude. We concede that this departure
147 from the RELM tradition (Schorlemmer & Gerstenberger, 2007) may also have disadvantages,
148 although the only one now apparent is the need for caution in the selection of testing
149 algorithms, as detailed in our electronic supplement.

150 HYBRID FORECASTS

151 The forecasts discussed in this paper do not include any explicit time-dependence. (However,
152 forecasts prepared using different calibration time windows will differ slightly as a result.) . All
153 forecasts have only a single depth bin: hypocentroids no more than 70 km below sea level. In
154 the form which we will retrospectively test (below), they have only a single magnitude bin: all
155 earthquakes at or above a magnitude threshold, without distinction. All forecast rate densities
156 are expressed on a common global grid of $0.1^\circ \times 0.1^\circ$ cells, are uniform within each cell, and are
157 discontinuous at cell boundaries. We will refer to the Seismicity parent forecast as an $1800 \times$
158 3600 matrix of positive numbers S_{ij} which give the forecast rate density of shallow earthquake
159 epicentroids in the cell at row i and column j of this grid, in units of $\text{m}^{-2} \text{s}^{-1}$. (Because we use
160 seismicity rate density, the values are laterally smooth near the poles, instead of becoming very
161 small as they would if we tabulated expected earthquake numbers.) We will refer to the
162 Tectonics parent forecast as matrix T_{ij} , and to the Hybrid forecast as matrix H_{ij} . The rough or
163 initial version of each hybrid H''_{ij} is produced by parallel numerical operations on all
164 corresponding pairs of Seismicity (\tilde{S}) and Tectonics (\tilde{T}) cells, without any lateral interactions
165 between neighboring cells.

166 Another simplification in the first phases of this study was that we scaled the Seismicity forecast
167 to have the same global earthquake rate as the Tectonics forecast, before combining them.
168 That is, both parent forecasts followed the global frequency/magnitude curve of the Tectonics
169 forecast, which in turn was based on the union of different tapered Gutenberg-Richter
170 distributions (Bird & Kagan, 2004) for different plate-boundary analogs. This approach is not

171 necessarily the best for scaling to higher threshold magnitudes, and in a later section below, we
 172 will propose a potentially more accurate (but more complex) solution. However, because the
 173 algorithms that we will use for scoring forecasts are insensitive to overall forecast earthquake
 174 rate, this choice of scaling method has little or no effect on our test results.

175 To obtain the final form H_{ij} of each hybrid forecast we apply two regularizing transformations,
 176 the second of which introduces some weak lateral interaction. First, we require that every cell
 177 of every hybrid have a positive value, no less than a minimum epicentroid-rate-density value f ,
 178 which we have chosen as $f = \inf(\inf(S_{ij}), \inf(T_{ij}))$, where “inf” stands for “infimum” (the lesser, as
 179 in the intrinsic MIN function of Fortran):

$$180 \quad H'_{ij} = \sup(H''_{ij}, f) \quad (1)$$

181 and “sup” stands for “supremum” (the greater, as in the intrinsic MAX function of Fortran).

182 Second, we normalize the global integral of the forecast to a desired global shallow earthquake
 183 rate R , while preserving minimum seismicity density f , by a linear transformation:

$$184 \quad H_{ij} = f + (H'_{ij} - f)(R - Gf) / ((\sum \sum H'_{ij} A_i) - Gf) \quad (2)$$

185 where A_i is the area of each cell in row i , and $G = 4\pi r^2 = 3600 \sum A_i$ is the area of the Earth based
 186 on a spherical approximation with radius r . We will abbreviate this second step by representing
 187 it as application of a normalizing forecast operation $H = N(H')$, and abbreviate the result of both
 188 regularizing steps by $H_{ij} = N(\sup(H''_{ij}, f))$. For all retrospective tests, the global earthquake rate
 189 R imposed by the $N()$ operator was chosen to be the same as that of both parent forecasts.

190 One traditional hybrid is a weighted linear-combination of S and T:

191
$$H_{ij} = N(\text{sup}((c S_{ij} + (1 - c) T_{ij}), f)) \quad (3)$$

192 where c is to be determined. Linear mixing of forecasts can be justified by either of two
193 arguments: (a) the two parent forecasts can be regarded as expressing alternative
194 measurements of the same underlying process, possibly with different error sources; or (b)
195 seismicity can be regarded as the sum of two independent components, which are described by
196 the Seismicity and Tectonics parents, respectively. Marzocchi *et al.* (2012) presented a complex
197 algorithm that could be used to estimate c . However, since there is only one parameter to
198 optimize, we prefer to create and test alternative hybrids using multiple values of c .

199 Another possible view might be that the two parent forecasts capture *independent*
200 prerequisites for seismicity: there must be a continuing energy source for lithospheric
201 deformation (some of which is elastic), *and* there must also be triggering by sudden stress
202 changes (either static or dynamic) due to nearby earthquakes to start a new earthquake
203 rupture. Probability theory predicts that the chance of an event requiring two independent
204 preconditions is proportional to the product of their two separate probabilities. Also, when
205 space/time discretization is fine enough so that all probabilities are much less than unity, then
206 rates are proportional to probabilities. Therefore, it is plausible to suppose that earthquake
207 rates might be proportional to the product of two precondition probabilities which might be
208 captured in the Seismicity and Tectonics forecast maps, respectively. In this view, it is more
209 appropriate to *multiply* the S and T estimates:

210
$$H_{ij} = N(\text{sup}((S_{ij}^d T_{ij}^{(1-d)}), f)) \quad (4)$$

211 or equivalently,

212
$$H_{ij} = N(\text{sup}((10^{d \log S + (1-d) \log T}), f)) \quad (5)$$

213 where d is an exponent to be determined. This set of hybrids will be called “log-linear.” Note
214 that $d = 0.5$ gives the geometric mean of Seismicity and Tectonics. We have only considered
215 exponents which sum to unity because the parent forecasts have each already been optimized
216 to contain the proper dynamic range of seismicity densities, and we want all log-linear hybrids
217 to share this property.

218 Finally, it is possible that both the Seismicity and Tectonics forecasts underestimate the true
219 rates in different localities, and so taking the larger of the two in every cell might more
220 successfully forecast future quakes. For example, the Tectonics forecast might underestimate
221 seismicity in regions of volcanism and landslides which lie in plate interiors, like Hawaii. The
222 Seismicity forecast may seriously underestimate the future seismicity of those plate-boundary
223 segments which happened not to have any large earthquakes during the learning period. So,
224 one additional hybrid selects the greater of Seismicity or Tectonics:

225
$$H_{ij} = N(\text{sup}(S_{ij}, T_{ij})) \quad (6)$$

226 Note that all hybrid models we produce use weights that are global and independent of
227 magnitude. Both spatially-variable weighting and magnitude-dependent weighting could be
228 considered in the future. The great difficulty lies in testing the value of such additional degrees
229 of freedom; if they only affect forecast rates of very rare earthquakes (*i.e.*, either at high
230 magnitudes, or in plate interiors), they are likely to remain untestable for centuries.

231 RETROSPECTIVE TESTING AGAINST EARTHQUAKES OF 2005-2012

232 The ideal way to evaluate success of forecasts is prospective testing by independent
233 authorities, such as the Collaboratory for the Study of Earthquake Predictability (CSEP).
234 However, since we intend to select a preferred model based on subtle differences seen in 8-
235 year retrospective tests, it could take a similar number of years to get definitive confirmation or
236 refutation of our selection. Also, to justify the effort of independent prospective testing,
237 models generally should demonstrate success in retrospective tests as a necessary (but not
238 sufficient) condition. Thus, we begin with retrospective tests. Of course, the largest 2005-2012
239 earthquakes are known to those who created the model, and this opens the door to subtle
240 biases. The tests we perform here might be called “pseudo-prospective” because we test
241 models that were created without using those years of the seismic catalog that will be used for
242 testing. However, we permit the use of other kinds of data, such as GPS velocities, that were
243 collected during the test years. This is because we use the GPS data to infer the secular or long-
244 term process, and the most recent data tend to be more accurate, permit the use of longer
245 time series, and are more geographically complete.

246 The primary test catalog we use is the full Global Centroid Moment Tensor (GCMT) catalog
247 (Ekström *et al.*, 2012, and references therein). It gives the location of the centroid (also known
248 as hypocentroid) which is the point source best representing the low-frequency and permanent
249 offsets due to one earthquake. For planar faults, this (hypo)centroid is typically located in the
250 middle of the slip distribution. We refer to the overlying surface point as the epicentroid.
251 GCMT is the catalog that was used for calibration in the Tectonics forecast and as a basis for
252 smoothing in the Seismicity forecast. Prior studies have shown it to be relatively complete

253 above scalar seismic moment $M = 10^{17.7}$ N m (Kagan, 2003). In this paper, we use the moment
254 (M)-to-magnitude (m) conversion of the U.S. Geological Survey:

$$255 \quad m = (2/3)(\log_{10}(M) - 9.05), \quad (7)$$

256 while noting that some other authors and authorities have used slightly different formulas, and
257 that some authors have preferred the symbols M_0 for scalar moment and M_w for magnitude.

258 Under conversion (7), $M = 10^{17.7}$ N m corresponds to moment magnitude $m = 5.767$.

259 The GCMT test period we use is 2005-2012 inclusive, or 8 full years. This yields 1694 shallow (\leq
260 70 km) test earthquakes (**Figure 2A**), but leaves the prior $\sim 78\%$ of the GCMT catalog available
261 for calibration and learning along each forecasting branch. Also, this test window postdates the
262 calibration study of Bird and Kagan (2004), who used years 1977-2003 of the GCMT catalog to
263 determine boundary half-widths, coupled thicknesses, corner magnitudes, and asymptotic
264 spectral slopes (β of Bird & Kagan, 2004) of different kinds of plate-boundary seismicity; all of
265 these determinations are employed in the Tectonics forecast under test.

266 The forecast-scoring metrics that we have used include the information scores I_0 (specificity)
267 and I_1 (success) of Kagan (2009), and the space statistic “ S ” of Zechar *et al.* (2010). The reasons
268 for selecting these metrics, and a general discussion of their algorithms and characteristics, can
269 be found in the electronic supplements to this article (see “Discussion of forecast-scoring
270 metrics”).

271 Because we will give the greatest weight to the I_1 (success) scores of the hybrid models when
272 we choose the preferred hybrid, an informal overview of this metric may be appropriate here.

273 I_1 is the mean (over all test-earthquakes) of the information gain (expressed as a number of

274 binary bits, including fractional bits) of the forecast under test, using the forecast relative
275 probability of the spatial cell into which the epicentroid of the test earthquake falls. The
276 reference model (for defining information gain) has equal seismicity spread uniformly across
277 the globe. Both the forecast under test and the reference model are expressed as maps of
278 conditional probability of the (longitude, latitude) location of the next test epicentroid, with
279 spatial integrals of unity; therefore, the overall rate of earthquakes forecast is not a factor in
280 any I_1 score; only the quality of its map-pattern is important. In our work, we have typically
281 found that the contributions to I_1 from individual test earthquakes range from about -5.8
282 (when the test earthquake is a surprise earthquake in a plate-interior) to about +10.5 (when the
283 test earthquake occurs in one of the most seismic subduction zones). Mean I_1 scores (averaged
284 over all test earthquakes during the test time window) range from about 3.4 to 4.3 for the
285 models rated here. Thus, the best results we discuss have mean forecast earthquake
286 probabilities (in the cells containing the actual test earthquakes) that are about $2^{(4.3-3.4)} = 2^{0.9} =$
287 1.866 times higher (87% higher) than in the worst results. Yet, even the worst model is better
288 by a mean factor of $2^{3.4} = 10.6$ than pure ignorance. The S statistic that we discuss and present
289 in our electronic supplements uses a totally different algorithm, but we found that it gave
290 similar or identical rankings of our hybrid forecasts. In contrast, the I_0 (“specificity”) metric of
291 Kagan (2009) is an abstract measure of the potential information gain of a forecast, computed
292 without regard to (*e.g.*, perhaps in advance of) any test earthquakes.

293 The threshold magnitude for our preferred test is the estimated catalog-completeness
294 threshold of $m \geq 5.767$ (Kagan, 2003; note our equation 7), because this yields the greatest
295 number of test earthquakes (1695) and so the greatest statistical power. We will abbreviate

296 this threshold as $m5.767+$ in supplementary tables (available in the electronic supplement to
297 this article) and in discussions. But, it is also important to learn whether the forecasts perform
298 equally well for larger, more damaging earthquakes. Therefore, we also perform parallel tests
299 on forecasts prepared using moment threshold $M \geq 3.548 \times 10^{19}$ N m (magnitude threshold $m \geq$
300 7.00 , or $m7+$). Unfortunately, at this level there are only 90 test earthquakes available, and the
301 statistical power of these tests is much lower. Testing at higher thresholds (*e.g.*, $m8+$ or $m9+$)
302 will not be meaningful for at least a century, even for the globe as a whole.

303 Results of all measures of forecast success and specificity for these GCMT tests are shown in
304 **Table S1**, available in the electronic supplement to this article. The variations of I_0 (specificity)
305 and I_1 (success) scores for all linear-combination and log-linear models are shown in **Figure 3**.
306 Four broad conclusions are apparent from Table S1 and from Figure 3:

307 1. Each method of hybridization we tried resulted in hybrids that score better than the parent
308 forecasts. This is true whether we measure success by I_1 or S . We suspect this occurs because
309 our two parent forecasts are very different, and reflect nearly independent approaches to
310 forecasting seismicity, with substantially uncorrelated biases and errors.

311 2. The log-linear mixing method produced the most successful hybrid, which was the one with d
312 $= 0.6$; that is, exponent of 0.6 on the Seismicity component and exponent of 0.4 on the
313 Tectonics component. This preferred hybrid will be referred to as H^* below. We suspect that
314 multiplicative mixing outperformed linear mixing because our two parent forecasts capture
315 independent requirements for seismicity: secular accumulation of elastic strain (Tectonics), and
316 time-specific triggering or advancement of slip instabilities (Seismicity). Future prospective

317 testing will be the best way to determine whether a log-linear hybrid is always superior to a
318 linear hybrid; we do not claim this as a definitive result.

319 3. The success of H^* at threshold $m5.767+$ seems hold up as the threshold is raised to $m7+$. (Its
320 S-statistic drops from 0.97 to 0.59, but the latter result is still excellent.) Naturally, the higher-
321 magnitude results are less definitive due to the limited number of test earthquakes. Still, this
322 encourages us to propose H^* as a viable candidate model for higher magnitudes, even though
323 forecasts for threshold magnitudes $m8+$ and $m9+$ cannot be conclusively tested with current
324 catalogs.

325 4. Hybridization, by any of the three methods we tested, results in lower specificity (I_0) of the
326 hybrid forecast, compared to the parents. This is natural, as each parent forecast predicts
327 moderate seismicity in a few regions which are at the intraplate-background level in the other
328 forecast. The loss of specificity is less with log-linear mixing than with the other two methods
329 we tried. The specificity I_0 of H^* is 3.801 for $m5.767+$, which is only slightly less than the 3.829
330 specificity of its Seismicity parent.

331 In selecting our preferred hybrid model (H^*), we gave primary weight to the I_1 success scores,
332 which measure the mean (over all test epicentroids) number of binary bits of information gain
333 from using this forecast instead of a spatially-uniform null forecast: this was about 4.2 bits at
334 both thresholds. We note that H^* also has the highest S-statistic in each set of tests (0.971 for
335 $m5.767+$, 0.59 for $m7+$). Specificity I_0 was not a selection criterion, because specificity
336 exceeding success is not particularly desirable, and suggests some systematic problem with a
337 forecast. However, we see (in Table S1, available in the electronic supplement to this article)

338 that very little specificity was sacrificed in preferring H^* relative to the Seismicity parent
339 forecast.

340 SIGNIFICANCE OF HYBRID IMPROVEMENT

341 An important question is, whether the improvement we have obtained through hybridization is
342 significant, considering the inherent time-variability of forecast scores? Can we show, in
343 advance of prospective testing, that our identification of the best model is likely to be stable,
344 and therefore that our preferred model H^* is truly superior? Actually, it is not very helpful just
345 to estimate the variance of each test metric individually; it is more useful to know their
346 correlations and the statistics of their differences. Here we argue that the difference is
347 significant, based on the small amount of time-history available to us and a simple scaling
348 argument. We focus on I_1 success, as it is the simpler measure to interpret. First, we look at
349 the year-to-year behavior of the critical score difference, and estimate its standard deviation
350 based on 8 test windows of one-year length. Then, we consider how standard deviations of
351 scores are expected to scale with the length of the test window; for this we appeal both to
352 theory and to the 36-year GCMT history of retrospective success of the Tectonics parent. This
353 leads to model standard deviations for our identified improvements in 8-year I_1 tests, and thus
354 an educated guess as to their significance.

355 **Table S2**, available in the electronic supplement to this article, shows the time-history through
356 2005-2012 of I_1 success scores of the preferred hybrid H^* and of the previous best parent
357 forecast, which was Seismicity. These annual tests with threshold $m5.767+$ used an average of
358 212 earthquakes per test. The time-history of the difference $I_1(H^*) - I_1(S)$ had a mean of 0.294

359 and a sample standard deviation of 0.087 across these one-year tests. The sample correlation
360 coefficient of the I_1 successes of these two forecasts is 0.958. This happens because some
361 years (*e.g.*, 2008) had several (4~5) unexpected intraplate earthquakes which lowered the
362 scores of both models, while some years (*e.g.*, 2011) had only ~1 intraplate earthquake, but had
363 many earthquakes on known plate boundaries which both models correctly forecast. This
364 finding is encouraging, because it suggests that meaningful distinctions between competing
365 models can be made after brief tests. For example, if the long-term average of the difference
366 $I_1(H^*) - I_1(S)$ is actually 0.294, as we currently estimate, and if this difference has a normal
367 distribution with standard deviation 0.087 across one-year tests, then the chance of finding a
368 negative difference (*i.e.*, preferring the other model) in any future one-year test would be less
369 than 0.1%, because such a result would be more than 3 apparent standard deviations from the
370 apparent mean of the difference.

371 If the threshold is raised to $m7+$ so that there are only ~11 earthquakes per test, then all results
372 are more variable and uncertain. These 8 one-year tests on the right side of Table S2 (available
373 in the electronic supplement to this article) show that standard deviations of the I_1 scores of
374 these two competing models rise by factors of 2.3 and 3.1, respectively, and the standard
375 deviation of their difference rises by a factor of 3.6, to 0.32. Still, the correlation of $I_1(H^*)$ with
376 $I_1(S)$ remains high, at 0.947. Consequently, the sign of the score difference $I_1(H^*) - I_1(S)$ only
377 reversed in one of the 8 years. Formally, we can estimate that, if the long-term mean score
378 difference is actually 0.47, and its standard deviation is actually 0.32 across multiple one-year
379 tests, then we would expect to see a preference for the Seismicity model (relative to the hybrid
380 H^*) in just 7% of one-year tests at threshold $m7+$.

381 The I_1 scores in Table S1 (available in the electronic supplement to this article) are even more
382 reliable for indicating relative model quality, because they are all from 8-year tests. We can
383 estimate the improvement in certainty by estimating how the standard deviations of score
384 differences scale with the number of years in the test. One might suppose that the standard
385 deviation of any test metric (or difference in metrics) should scale in proportion to $N^{-1/2}$, where
386 N is the number of test earthquakes. Of course, this can only be proven under the assumption
387 that earthquakes are independent. Also, scaling with number of earthquakes can only be
388 translated into scaling with number of years if earthquakes occur at a constant global rate.
389 Therefore, the simple hypothesis that standard deviations of test metrics should scale as $W^{-1/2}$,
390 where W is the length of the test time window, needs to be checked. **Figure 4** displays the
391 standard deviation of the I_1 success of the Tectonic parent forecast over the whole GCMT
392 period of 1977-2012; to obtain these small-sample standard deviations the 36-year history was
393 subdivided many times, into shorter windows with $W = 1$ yr, 2 yr, 3, yr, ... 9 yr, and these
394 windows were created using every possible start-year. (To obtain these bootstrap estimates,
395 we overlook the slight circularity of testing the Tectonics forecast against some of the same
396 earthquakes that were used to calibrate its 5 zonal seismicity-correction factors, as described
397 by Bird & Kreemer, 2015.) In fact, $W^{-1/2}$ scaling seems consistent with our results. This was
398 expected based on Kagan's (2009; his Fig. 3) result, using simulated catalogs rather than real
399 ones, that the I_1 score is a random variable whose distribution is close to a normal distribution.
400 Based on this scaling, we estimate that the standard deviations of the critical score difference
401 $I_1(H^*) - I_1(S)$ over multiple future 8-year tests should be 0.031 at threshold $m5.767+$ and 0.11
402 at threshold $m7+$. This means that the hybrid improvements in I_1 that we found in 8-year tests

403 (Table S1, available in the electronic supplement to this article) have signal/noise ratios of 9.5
404 (at threshold $m5.767+$) and 4.3 (at $m7+$).

405 Finally, we are able to assess the “statistical significance” of hybrid improvement, using first the
406 physical-sciences and then the statistical meaning of that term. Fortunately, both communities
407 share some common concepts and vocabulary: Our null hypothesis is that preferred hybrid H^*
408 is no better than the parent Seismicity forecast according to the I_1 metric. Our complementary
409 hypothesis is that H^* is better than Seismicity according to the I_1 metric. The p value is the
410 model chance of obtaining the actual signal/noise ratio (or a higher one) if the null hypothesis
411 were correct; it is obtained from the Gaussian cumulative distribution function (with mean of 0
412 and standard deviation of 1) when the independent variable is the negative of the signal/noise
413 ratio, so in this case $p = 1 \times 10^{-21}$ (at $m5.767+$) and $p = 8.5 \times 10^{-6}$ (at $m7+$). The complement of
414 the p -value is $(1 - p)$.

415 In physical-sciences usage, “statistical significance” is a positive real number, expressed using
416 any of 3 popular metrics: signal/noise ratio, p -value, or the complement of the p -value
417 (often described as %-confidence). The significance level is considered to be p . Therefore we
418 can say, in physical-science usage, that there is more than 99%-confidence that hybrid
419 improvement is real, at either magnitude threshold.

420 In statistical usage, “statistical significance” is limited to the logical values True or False. To
421 determine which is appropriate requires a pre-selected significance level based on community
422 standards. For purposes of illustration, let us select $\alpha = 0.01$. Then, the statistical significance
423 of hybrid improvement is True at either threshold, because both p -values are less than α .

424 RETROSPECTIVE TESTING AGAINST EARTHQUAKES OF 1918-1976

425 Storchak *et al.* (2012) released the International Seismological Centre-Global Earthquake Model
426 (ISC-GEM) catalog, which is a comprehensive revision of the longstanding ISC catalog. Their
427 work included consultation of original sources; inclusion of more phases; uniform relocation of
428 all earthquakes with a single modern algorithm; and assignment of moment magnitude (m) to
429 every event, either through review of the literature or by use of regression relations. This new
430 catalog is believed to be relatively complete for moment threshold $M \geq 1.778 \times 10^{19}$ N m ($m6.8+$)
431 from 1918 onward (Michael, 2014; Di Giacomo *et al.*, 2015). In those years which predate the
432 routine production of GCMT solutions (1918-1976), there are 881 shallow earthquakes of
433 $m6.8+$ in this catalog which we have not previously used, either for model-construction or for
434 testing. We take this opportunity to assess whether the hybrid improvements that we
435 demonstrated in the previous sections are specific to the last decade and to the GCMT catalog,
436 or are more universal.

437 Parent and hybrid models were prepared for threshold $m6.8+$, but otherwise in exactly the
438 same ways as for the previous tests. That is, the catalog-calibration window for both parents
439 was GCMT 1977-2004.

440 **Table S3**, available in the electronic supplement to this article, gives all of these test results.

441 The patterns we see are almost identical to those from $m7+$ tests against GCMT 2005-2012
442 (Table S1), except that these tests have more statistical power due to 10 times as many test
443 earthquakes, and that I_1 successes and S-statistics are generally lower. As before, we find that:
444 (1) Both parent forecasts have comparable success; (2) All hybrid forecasts perform better than

445 either parent, with a maximum improvement of +0.4 in I_1 ; (3) Log-linear hybrids perform best;
446 (4) The best log-linear hybrid is a relatively even blend of Tectonics and Seismicity; and (5) The
447 loss of I_0 specificity for the H* preferred hybrid, relative to the Seismicity parent, is small.

448 These results are important because they demonstrate that the value of each parent forecast,
449 and the improvement in hybrid mixtures, is relatively independent of time and technology. The
450 generally lower level of I_1 success scores (offset by -0.4) and S-statistics (offset by -0.23)
451 compared to the GCMT 2005-2012 tests in Table S1 (available in the electronic supplement to
452 this article) can probably be attributed to two causes: (1) There are less accurate epicenters,
453 depths, and magnitudes in the ISC-GEM catalog. Even though events have been relocated with
454 modern algorithms, errors in phase arrival times due to analog recording and/or clock drift in
455 the period 1918-1976 are much more difficult to correct. Also, accurate magnitude estimation
456 is difficult with narrow-band seismometers, and (in the early decades) with non-standard
457 seismometers. (2) The Seismicity parent forecast gets less help from long-running aftershock
458 sequences when the test window is longer.

459 SCALING THE SEISMICITY PARENT FORECAST TO HIGH MAGNITUDES

460 The previous discussion has focused entirely on testing and optimizing the map-patterns of
461 forecasts at those moderate magnitudes where test earthquakes are abundant. Yet, the high-
462 resolution global forecast template of CSEP requires estimation of earthquake rate maps at
463 thresholds up to $m8.95+$. Also, the GEM Foundation has a goal of building global seismic hazard
464 and risk models which will require similar high-magnitude rate estimates. Computation of a
465 preferred hybrid forecast H* for a high threshold magnitude requires that we have

466 corresponding versions of both parent forecasts. Since the high-magnitude scaling of the
 467 Tectonics forecast is already defined (Bird and Kreemer, 2015), it remains to specify how the
 468 Seismicity parent forecast will be extrapolated to high magnitudes. To reduce artifacts and
 469 problems, it is important to take account of the different corner magnitudes m_c (which locate
 470 the roll-offs of frequency/magnitude curves) in different tectonic settings (Bird *et al.*, 2002; Bird
 471 & Kagan, 2004; Kagan *et al.*, 2010).

472 A straightforward way to incorporate this information is to scale the local (per-cell) epicentroid
 473 rate densities, from the original Seismicity forecast with threshold $m_t = 5.767$ to a higher
 474 threshold m (*e.g.*, 8), by use of the G factor from the tapered Gutenberg-Richter frequency-
 475 moment relation:

$$476 \quad \frac{S_{ij}(m)}{S_{ij}(m_t)} = G(m, m_t, m_c, \beta) = \left(\frac{M(m)}{M(m_t)} \right)^{-\beta} \exp\left(\frac{M(m_t) - M(m)}{M(m_c)} \right) \quad (8)$$

477 where the $S_{ij}(m)$ are per-cell shallow earthquake rate densities (in $m^{-2} s^{-1}$) above magnitude m ;
 478 $M(m)$ is the scalar moment associated (7) with magnitude m ; m_c is the corner magnitude in the
 479 cell, and β is the asymptotic spectral slope of the frequency-moment relation (for $m \ll m_c$) in
 480 the same cell (Jackson & Kagan, 1999; Kagan & Jackson, 2000; Bird & Kagan, 2004).

481 We first implemented scaling (8) using the maximum-likelihood corner magnitudes (6.79 ~ 8.75)
 482 and spectral slopes (0.639 ~ 0.767) of the 5 tectonic zones in Table 1 of Kagan *et al.* (2010),
 483 together with the tectonic-zone map of the same paper. After a number of experiments, we
 484 decided to moderate this simplistic application of tectonic zonation in five ways: [1] We raised
 485 the corner magnitude of zone 4 (Trench) to 9.5, based on later research of Kagan & Jackson

486 (2013). This value is also more consistent with results of Bird & Kagan (2004); yet it still falls
487 within the uncertainty of Kagan *et al.* (2010). [2] We merged tectonic zone 0 (Intraplate) with
488 tectonic zone 1 (Active continent) using weighted-averages $m_c = 7.72$ and $\beta = 0.645$ in their
489 union, in order to eliminate artifacts which had been appearing along the 0/1 zone boundaries
490 during extrapolation. These two mean values are within the uncertainty ranges of the 4
491 unmerged estimates in Kagan *et al.* (2010). [3] We spatially smoothed the map of zone-based
492 corner magnitude and the map of zone-based spectral slope to eliminate remaining
493 discontinuities; this smoothing is done by convolution with an isotropic Gaussian kernel of scale
494 length 200 km. [4] We applied a constant stretching factor to variations from the mean within
495 each smoothed map, in order to restore their original standard deviations. (Before smoothing,
496 corner magnitudes had an area-weighted mean of 7.806 and standard deviation of 0.463;
497 smoothing reduced this standard deviation to 0.322; amplification of remaining variations by
498 factor 1.439 brought the standard deviation back to 0.463.) [5] During extrapolation of the
499 Seismicity forecast to high magnitudes, we applied the extrapolated epicentroid rate density of
500 the united zone 0/1 (outside the halos of any catalog earthquakes) as a lower limit on the
501 forecast epicentroid rate density of all cells. This is to recognize the possibility of occasional
502 energetic ruptures on new faults, even in the vicinity of old plate boundaries. It also limits the
503 dynamic range of the extrapolated forecast to be more similar to the dynamic range of the
504 forecast for $m_{5.767+}$ which was previously optimized, and which we have tested. Details of this
505 algorithm are contained in the source code provided as an electronic supplement to this article.
506 **Figure 5** shows an example of a Seismicity parent forecast (for years 2005+) extrapolated to
507 m_{8+} by these methods.

508 The extrapolated Seismicity parent forecast is now in reasonable agreement with the
509 frequency-magnitude statistics of global catalogs (**Table 1**). However, this exercise highlighted
510 the importance of both the corner magnitude we apply in zone 4 (Trench), and the generic
511 frequency/magnitude curve that we assumed for all zones. Great $m9+$ earthquakes are rare, a
512 few per century, and the rate difference, if we accept $m_c = 9.5$, between a straight-line
513 Gutenberg-Richter frequency/magnitude distribution and a tapered Gutenberg-Richter
514 distribution seems small. As calculated previously (Jackson & Kagan, 2012; Kagan & Jackson,
515 2013), the global rate of $m10+$ events is 0.057 per century or 0.21 per century for the gamma
516 distribution or tapered Gutenberg-Richter distribution, respectively. But, it increases to 0.57 per
517 century for the classical straight-line Gutenberg-Richter law. We recognize the desirability of
518 further research and testing regarding these issues.

519 GLOBAL EARTHQUAKE ACTIVITY RATE MODEL

520 Earlier in this paper we established that the best-performing hybrid H^* in the most powerful
521 retrospective test (against shallow GCMT earthquakes, $m5.767+$, in 2005-2012) was the log-
522 linear hybrid (equations 4, 5) with exponent of $d = 0.6$ on the Seismicity component. This gives
523 us a basis for proposing a global reference model that presently appears optimal, at least for
524 those moderate magnitudes where testing is currently meaningful. However, the earthquake
525 rates of the two parent forecasts diverge slightly at high threshold magnitudes; thus, we must
526 also specify a choice regarding the combination of these two forecasts of the global shallow
527 earthquake rate (R_s from Seismicity; R_T from Tectonics) for $m > 5.767$. By analogy with the
528 formula that determines the map-pattern of H^* , we choose the global rate formula

529
$$R_{H^*}(m > 5.767) = R_S^{0.6}(m) \times R_T^{0.4}(m). \quad (9)$$

530 Up until this point, we have illustrated, tested, and discussed models based on GCMT catalog
531 years 1977-2004, which left the years 2005-2012 (and 1918-1976) available for testing. To
532 improve our preferred model in advance of prospective testing, it is also important to make use
533 of all available years in the modern broad-band digital-seismology catalog. Thus, we
534 recomputed both parents, Seismicity and Tectonics, and the preferred hybrid H* based on all
535 available complete GCMT years: 1977-2013. One change was that $R_{GCMT}(5.767)$ based on 1977-
536 2013 is 6.5% higher than the rate based on 1977-2004 (Figure 2) because of the rate increase of
537 26.7% that occurred at the end of 2004. Another change was that local maxima in forecast
538 seismicity appear near large earthquakes of 2005-2013 because of the influence of the updated
539 Seismicity parent forecast.

540 This update of our preferred hybrid model H*, with $R_{H^*}(m>5.767)$ based on (9) above, is named
541 Global Earthquake Activity Rate model 1 (GEAR1). Figure 2B and **Figure 6** show maps of this
542 model at thresholds of $m5.767+$ and $m8+$, respectively. As threshold magnitude rises above the
543 calibration level of $m5.767+$, GEAR1 global earthquake rates forecast for the future match past
544 instrumental catalog rates fairly well through thresholds $m7+$, $m8+$, and $m9+$ (Table 1).

545 There are a number of reasons why GEAR1 will eventually be superseded by revised versions
546 (“GEARn”). Continuing enlargement of the global GPS dataset may eventually prompt an
547 update of the Tectonics parent component. Also, an improved hybrid might use a future
548 Tectonics forecast employing both GPS strain-rates and the GEM Faulted Earth and/or GEM
549 Subduction Sources datasets in a unified kinematic finite-element deformation model. The

550 extrapolation of the Seismicity parent forecast to high magnitudes may be revised or further
551 optimized. Catalog seismicity from before 1977 may eventually be incorporated into the
552 Seismicity parent forecast. Also, strong seismicity in risk-sensitive parts of the globe could
553 prompt an update of the Seismicity component, again leading to a new GEAR. In any case,
554 long-term independent prospective testing of GEAR1, whether superseded or not, should have
555 value in verifying the expected long-term stability of hybrid improvement.

556 In the CSEP forecast format (XML file), all forecasts must have defined start- and end-dates.
557 The forecast start-date and end-date for GEAR1 must be chosen by the user, in the
558 GEAR1_parameters.dat file which is input before the XML file is created. The start-date should
559 be no earlier than 2014.01.01 to avoid circularity. All forecast earthquake counts in each
560 magnitude bin of each spatial cell will be proportional to the length of the forecast time
561 window. However, conceptually the time-window for this GEAR1 forecast is 2014+, which is
562 indefinite or open. (This is why we prefer to display our results as maps of earthquake rates
563 rather than earthquake counts.)

564 An important question for future testing and research is: For how long into the future should a
565 forecast of the GEAR type be trusted? Large earthquakes (especially those in unexpected
566 places) modify the forecast map of the Seismicity parent forecast, and thus any GEAR forecast;
567 however, after their aftershocks have died out, it might be a very long time until the next large
568 earthquake in that area. Thus, it is conceivable that very-long-term seismicity (*e.g.*, 100 years
569 into the future) might be overpredicted in some intraplate regions. This is an open question, as
570 many previous seismic-hazard models, created in other ways, have also anticipated elevated
571 hazard for two or more centuries following famous historic earthquakes. By omitting any

572 stated expiration-date for the current GEAR1 forecast, we do not mean to guarantee that there
573 is no such date; we only note that this is a complex question which cannot yet be answered.

574 USE OF GEAR1 FOR CATASTROPHE BONDS

575 GEAR1 can easily be used to calculate the earthquake magnitude for which there is a 1% (or
576 any) annual probability of occurrence in circles of 100-km (or any) radius, and so can be used to
577 estimate the risk of triggering a parametric catastrophe bond (Franco, 2010) payment based on
578 this criterion. A global map of this type is shown in **Figure 7**. If the radius of integration circles
579 were increased, all magnitudes would rise. Importantly, this map refers to epicentroids, rather
580 than ends of ruptures which might, or might not, extend into a given integration circle. On the
581 basis of published USGS procedures, authoritative earthquake centroid locations and
582 magnitude assignments are routinely reported for global earthquakes by the USGS 'ComCat'
583 within minutes to hours, and are fixed and finalized six weeks after the mainshock. Thus, both
584 the estimate of the likelihood of the trigger, and the timely confirmation of its occurrence, can
585 be fully, unambiguously, and transparently specified.

586 GEAR1 could therefore serve as a basis for catastrophe bonds, in which investors receive a high
587 rate of interest on their principal until and unless the specified earthquake strikes, in which case
588 they would lose their principal. A GEAR-based bond could open the market to quake-
589 threatened developing nations, and creating new and more diversified opportunities for
590 investors. There could be composite global bonds, or many smaller bonds or reinsurance
591 securities customized for the regions of interest to investors (those taking the risk) and cedants

592 (those reducing their risk). Ultimately, GEAR1 could be an efficient and transparent platform
593 for the exchange of financial risk.

594 COMPARISON TO REGIONAL FORECASTS: California

595 One purpose of this global seismicity model is to provide first-order estimates of seismicity in
596 regions that lack their own regional seismic-hazard programs. Another purpose is to initiate
597 comparisons with detailed national and regional models created by other methods. Naturally,
598 many seismologists will regard these comparisons as tests of GEAR1. We advocate a more
599 neutral approach: Large differences between GEAR1 and regional forecasts (if not readily
600 explained by differences in format or data scope, or simple explanations based on the temporal
601 limitations of GEAR) should lead to further investigation of both GEAR1 and these other
602 independent forecasts. In any case, future prospective testing of these competing forecasts
603 should be conducted because of its very low marginal cost.

604 Our GEAR1 forecast does not use any database of active faults. However, many regional
605 models do use fault traces, and sometimes associated slip rates. Thus, one expected difference
606 is that the GEAR1 forecast is likely to be spatially smoother, and lack sharp maxima along traces
607 of active faults. The Tectonics parent of the GEAR1 forecast was based on an approximation
608 (Bird & Kreemer, 2015) that secular strain-rates recorded by GPS (or implied by relative plate
609 rotation) are good proxies for long-term tectonic strain; however, interseismic elastic strain
610 accumulation is known to be spatially smoother than eventual seismic strain release. The
611 Seismicity parent of the GEAR1 forecast is also necessarily smooth because its source catalog
612 (GCMT, *m*5.767+, 1977-2013) only captures a modest number of earthquakes in most regions,

613 and these point sources must be spatially smoothed to provide an optimized forecast of future
614 seismicity. For example, in the California-centric rectangle defined by limits [$126^{\circ}\text{W} \leq \text{longitude}$
615 $\leq 114^{\circ}\text{W}$] and [$32^{\circ}\text{N} \leq \text{latitude} \leq 42^{\circ}\text{N}$], only 52 such earthquakes have been recorded by GCMT.
616 Because of this contrast in resolution, it may be most valuable to compare overall seismicity
617 rates and patterns of low spatial frequency (such as those obtained by smoothing the detailed
618 regional forecast).

619 Another expected difference is that many regional models refer to past earthquakes inferred
620 from analog-instrumental catalogs, from historical catalogs, or from paleoseismic field studies.
621 But GEAR1 uses no data regarding events before 1977. In the U.S.A., a prominent example is
622 that the National Seismic Hazard Maps (*e.g.*, Petersen *et al.*, 2008) show high forecast hazard
623 around the epicenters of the 1811-1812 earthquakes in the area of New Madrid, MO, but
624 GEAR1 does not forecast high seismicity there. In such cases, a higher forecast seismicity in the
625 regional model is easily understood, although it is still subject to prospective testing. However,
626 any difference in which the regional model projects a lower overall seismicity than GEAR1
627 should be investigated; it may be found to depend critically on a questionable assumption.

628 Here we present a brief comparison of GEAR1 to the Unified California Earthquake Rupture
629 Forecast version 3 (UCERF3) of Field *et al.* (2013) which is widely considered to be one of the
630 most technically complex regional forecasts. This model used an expanded database of active
631 faults, not limited to faults with measured geologic slip rate. Its logic-tree considered 4
632 alternative deformation models, with 70% total weight on a set of 3 kinematically self-
633 consistent deformation models that merged geologic, geodetic, and plate-tectonic constraints.
634 Also, it simulated the earthquake-rupture process in detail in order to include multi-fault

635 ruptures, creating thousands of virtual catalog realizations, constrained by seismic catalogs,
636 fault slip rates from the deformation models, and geologic recurrence intervals. Both forecasts
637 of long-term epicentroid rate density are presented for comparison in **Figure 8**. The GEAR1
638 forecast has been windowed to display only the area of $7.50 \times 10^{11} \text{ m}^2$ that is also covered by
639 UCERF3.

640 At magnitude threshold $m5.8+$, these two forecasts anticipate very similar total earthquake
641 rates: 121 epicentroids/century in GEAR1, and 126 epicentroids/century in UCERF3. The
642 UCERF3 forecast has higher spatial variance; if we divide the spatial standard deviation of each
643 forecast by its respective mean rate, these relative standard deviations are 155% for GEAR1 but
644 181% for UCERF3. Consistent with this, the I_0 specificities are 0.896 for GEAR1 (in the California
645 region of Figure 8) but 1.069 for UCERF3. Both statistics confirm the visual impression that the
646 UCERF3 forecast seismicity is more strongly concentrated along traces of modeled faults. The
647 correlation coefficient between these two forecasts is 0.482. However, we also tried smoothing
648 the UCERF3 forecast and then re-computing correlations of these smoothed versions of UCERF3
649 with (unchanged) GEAR1; we found that the correlation coefficient rises smoothly to a
650 maximum of 0.625 when the smoothing is done by convolution with a 2-D Gaussian bell-curve
651 function of characteristic length 30 km. The specificity of this particular smoothed version of
652 UCERF3 would drop to 0.608, which is actually below the local specificity of GEAR1.

653 At threshold magnitude $m7.0+$, the results are similar. The spatially-integrated total rates are
654 7.64 epicentroids/century for GEAR1 and 7.49 epicentroids/century for UCERF3. The relative
655 standard deviation is stable at 159% for GEAR1, but rises to 224% for UCERF3. Specificity I_0 is
656 stable at 0.909 for GEAR1 (in California) but rises to 1.755 for UCERF3. Both of these statistics

657 indicate an even stronger concentration of UCERF3 seismicity on modeled faults at threshold
658 $m7+$. The correlation coefficient between the two models is 0.462, but this rises to a peak of
659 0.600 when the UCERF3 model is smoothed using a characteristic length of 25 km; this same
660 amount of smoothing would also lower the UCERF3 specificity to 1.024 which is not much more
661 than the local specificity of GEAR1.

662 Thus, these two forecasts have strong similarities, but the UCERF3 forecast provides a sharper
663 focus because it was based on traces of known active faults, while GEAR1 was not. The ideal
664 level of forecast smoothness is currently uncertain, and needs to be tested and optimized in
665 future prospective experiments. A formal prospective test of all recent California forecasts, also
666 including those of Marzocchi *et al.* (2012) and of Hiemer *et al.* (2013) and of Rhoades *et al.*
667 (2013, 2014), would be valuable, even though a lengthy duration (*e.g.*, 50~200 years) will
668 probably be required for conclusive ranking of all these models.

669 It is worth noting that the plausibility of GEAR1 seen in this California comparison may depend
670 strongly on the very widespread and precise network of GPS observations in the region, which
671 both models incorporate, although in different ways. Unless both of these forecasts are
672 contradicted by future seismicity, this comparison leaves an impression that geodetic
673 observation may partially substitute for full knowledge of active fault locations and rates, at
674 least for applications in which the precise locations of future ruptures are not required.

675 CONCLUSIONS AND PROSPECTS

676 This project has succeeded in merging disparate long-term seismicity models into testable
677 global forecasts of long-term shallow seismicity, and has made a start on testing them,

678 retrospectively. We find that multiplicative blends of smoothed-seismicity and tectonic
679 forecasts outperform linear blends. The improvement in information score is large, and quite
680 unlikely to be due to one-time random fluctuations in seismicity. It is encouraging that our
681 preferred model, though chosen for its improved performance in forecasting catalog years
682 2005-2012, also outperforms previous methods in forecasting catalog years 1918-1976.
683 Furthermore, a local comparison to the recent UCERF3 long-term forecast in California shows
684 that both anticipate the same overall earthquake rates, with the map-pattern of our GEAR1
685 model closely resembling a smoothed version of the map-pattern of UCERF3.

686 In the near future, this GEAR1 forecast will be submitted for independent prospective testing at
687 CSEP; preliminary results should be available after only one year of testing because of its global
688 scope. Assuming success similar to that we have seen retrospectively, others may wish to build
689 rupture models and seismic-hazard models based on GEAR1, by supplementing its maps of
690 epicentroid rate density with specific fault sources (where known) or focal mechanisms
691 (elsewhere), with rupture depths and extents, and with attenuation relations. It will be
692 important to add supplemental data (and/or assumptions) about the depths of shallow
693 ruptures; GEAR1 has made no distinctions between earthquakes within its depth range of 0~70
694 km because of the limitations of available test catalogs; however, a rupture model built from
695 GEAR1 would need to be more precise. It will also be important to make policy decisions
696 regarding whether historical and/or paleoseismic events (like those around New Madrid, MO in
697 the U.S.A.) should result in locally-elevated model hazard, despite the absence of complete and
698 consistent global databases of historical and/or paleoseismic events, and the absence of
699 rigorous prospective testing of related hypotheses. Another possibility for future development

700 is that the availability of transparent estimates of the occurrence of large shallow earthquakes
701 in specific local regions could contribute to greater trade in parametric catastrophe bonds.
702 Looking beyond GEAR1 to potential future versions, there is an opportunity for further
703 improvement by incorporating seismic catalog years before 1977 into the smoothed-seismicity
704 parent forecast, and by incorporating new geodetic data and revised plate models into the
705 tectonic parent forecast.

706 DATA AND RESOURCES

707 The source code and data files used to create the Tectonics parent forecast were described by
708 Bird and Kreemer (2015). These same data files are needed to compute the GEAR1 hybrid
709 model, although the application code is different. These file-names are listed in the small
710 parameter file GEAR1_parameters.dat (available in the electronic supplement to this article).

711 The only dataset used to compute the Seismicity parent forecast was the Global Centroid
712 Moment Tensor catalog. We provide this parent forecast, for years 2014 and after, as the large
713 (439 MB) ASCII table file GL_HAZTBLT_M5_B2_2013.TMP (available in the electronic
714 supplement to this article, in a compressed .zip format occupying 56 MB).

715 Our GEAR1 forecast is provided in the form of Fortran 90 source code GEAR1_for_CSEP.f90,
716 available in the electronic supplement to this article. This is an extension and expansion of
717 program SHIFT_GSRM2f_for_CSEP.f90 described and published by Bird and Kreemer (2015). A
718 compiled 64-bit executable for Windows is available from the first author. This program will
719 produce a 3.7 GB file containing a global grid of $0.1^\circ \times 0.1^\circ$ cells, with forecast shallow seismicity
720 of each cell divided into 31 magnitude bins ranging from $m = 6.00 \pm 0.05$ in steps of 0.10 up to

721 the final open-ended bin $m8.95+$, in the XML format required by CSEP. Utility program
722 XML_2_GRD, available from the web site of the first author, can be used to extract a spatial grid
723 for any desired threshold magnitude from $m5.75+$ to $m9.15+$. Another utility program,
724 extract_regional_GRD, can be used to extract a rectangular subregion at the same threshold
725 magnitude. GRD file format is documented at http://peterbird.name/guide/grd_format.htm
726 (last visited February 2015). The website of the first author also provides a mapping tool
727 (NeoKineMap) and two forecast-scoring tools (Kagan_2009_GJI_I_scores, and pseudoCSEP) that
728 work with this GRD file format, and which were used in this study to create maps and tables,
729 respectively.

730 ACKNOWLEDGEMENTS

731 Graeme Weatherill performed PSHA hazard calculations with a preliminary version of this
732 model, helping greatly to define its strengths and limitations. Mark Stirling organized a Powell
733 Conference on this model and advised on its construction, as did Martin Käser, Harold
734 Magistrale, Morgan Page, Yufang Rong, and Graeme Weatherill. Edward Field and Peter
735 Powers provided a gridded-seismicity forecast for the California region based on UCERF3.
736 Edward Field, Wayne Thatcher, Mark Stirling, and an anonymous reviewer provided thoughtful
737 reviews leading to clarification. We gratefully acknowledge the U.S. Geological Survey (USGS)
738 John Wesley Powell Center for Analysis and Synthesis, where the GEAR project received its first
739 external review, as well as financial support from the USGS, the Global Earthquake Model
740 (GEM) Foundation, the National Science Foundation (NSF), the Southern California Earthquake
741 Center (SCEC), and the University of California Los Angeles (UCLA). DDJ and YYK received

742 support from NSF through grants EAR-0944218 and EAR-1045876. This research was also
743 supported by SCEC, which is funded by NSF Cooperative Agreement EAR-1033462 and USGS
744 Cooperative Agreement G12AC20038. The SCEC contribution number for this paper is 2075.
745 Publication was supported by the USGS. All opinions, expressed or implied, are those of the
746 authors and do not reflect official positions of the USGS, GEM Foundation, NSF, SCEC, or UCLA.

747 REFERENCES CITED

- 748 Bird, P. (2009). Long-term fault slip rates, distributed deformation rates, and forecast of
749 seismicity in the western United States from fitting of community geologic, geodetic,
750 and stress direction datasets, *J. Geophys. Res.*, **114**, B11403, doi:
751 10.1029/2009JB006317.
- 752 Bird, P., and Y. Y. Kagan (2004). Plate-tectonic analysis of shallow seismicity: Apparent boundary
753 width, beta, corner magnitude, coupled lithosphere thickness, and coupling in seven
754 tectonic settings, *Bull. Seismol. Soc. Am.*, **94**(6), 2380-2399.
- 755 Bird, P., and C. Kreemer (2015). Revised tectonic forecast of global shallow seismicity based on
756 version 2.1 of the Global Strain Rate Map, *Bull. Seismol. Soc. Am.*, 105(1), 152-166, doi:
757 10.1785/0120140129.
- 758 Bird, P., and Z. Liu (2007). Seismic hazard inferred from tectonics: California, in: S. E. Hough and
759 K. B. Olsen (ed.), Special Issue on: Regional Earthquake Likelihood Models, *Seismol. Res.*
760 *Lett.*, **78**(1), 37-48.
- 761 Bird, P., Y. Y. Kagan, and D. D. Jackson (2002). Plate tectonics and earthquake potential of
762 spreading ridges and oceanic transform faults, in: S. Stein and J. T. Freymueller (editors),

763 Plate Boundary Zones, *Geodynamics Series*, **30**, 203-218, Am. Geophys. U., Washington,
764 DC.

765 Bird, P., Y. Y. Kagan, D. D. Jackson, F. P. Schoenberg, and M. J. Werner (2009). Linear and
766 nonlinear relations between relative plate velocity and seismicity, *Bull. Seismol. Soc.*
767 *Am.*, **99**(6), 3097-3113, doi: 10.1785/0120090082.

768 Bird, P., C. Kreemer, and W. E. Holt (2010a). A long-term forecast of shallow seismicity based on
769 the Global Strain Rate Map, *Seismol. Res. Lett.*, **81**(2), 184-194, plus electronic
770 appendices.

771 Bird, P., Y. Y. Kagan, and D. D. Jackson (2010b). Time-dependent global seismicity forecasts with
772 a tectonic component: Retrospective tests (abstract), *Eos Trans. Am. Geophys. U.*,
773 **91**(52), Fall Meeting Supplement, Abstract S44B-03.

774 Di Giacomo, D., I. Bondár, D. A. Storchak, E. R. Engdahl, P. Bormann, and J. Harris (2015). ISC-
775 GEM: Global instrumental earthquake catalogue (1900-2009), III: Re-computed M_S and
776 m_b , proxy M_W , final magnitude composition and completeness assessment, *Phys. Earth*
777 *Plan. Int.*, **239**(2), 33-47, doi: 10.1016/j.pepi.2014.06.005.

778 Ekström, G., M. Nettles, and A. M. Dziewonski (2012). The global CMT project 2004-2010:
779 Centroid moment tensors for 13,017 earthquakes, *Phys. Earth Planet. Inter.*, **200-201**, 1-
780 9.

781 Field, E. H. (2007). Overview of the Working Group for the Development of Regional Earthquake
782 Likelihood Models (RELM), in: S. E. Hough and K. B. Olsen (ed.), Special Issue on:
783 Regional Earthquake Likelihood Models, *Seismol. Res. Lett.*, **78**(1), 7-16.

784 Field, E. H., G. P. Biasi, P. Bird, T. E. Dawson, K. R. Felzer, D. D. Jackson, K. M. Johnson, T. H.
785 Jordan, C. Madden, A. J. Michael, K. R. Milner, M. T. Page, T. Parsons, P. M. Powers, B. E.
786 Shaw, W. R. Thatcher, R. J. Weldon, II, and Y. Zeng (2013). Unified California Earthquake
787 Rupture Forecast, version 3 (UCERF3)-The time-independent model, *U.S. Geol. Surv.*
788 *Open-File Rep.*, **2013-1165** (*Cal. Geol. Surv. Spec. Rep.* **228**, and *Southern California*
789 *Earthquake Center Pub.* **1792**), 97 pages; <http://pubs.usgs.gov/of/2013/1165/>.

790 Franco, G. (2010). Minimization of trigger error in cat-in-a-box parametric earthquake
791 catastrophe bonds with an application to Costa Rica, *Earthquake Spectra*, **26**, 983-998,
792 doi: 10.1193/1.3479932.

793 Hiemer, S., D. D. Jackson, Q. Wang, Y. Y. Kagan, J. Woessner, J. D. Zechar, and S. Wiemer (2013).
794 A stochastic forecast of California earthquakes based on fault slip and smoothed
795 seismicity, *Bull. Seismol. Soc. Am.*, **103**(2A), 799-810, doi: 10.1785/0120120168.

796 Jackson, D. D., and Y. Y. Kagan (1993). Reply [to Nishenko & Sykes], *J. Geophys. Res.*, **98**(B6),
797 9917-9920: doi: 10.1029/93JB00699.

798 Jackson, D. D., and Y. Y. Kagan (1999). Testable earthquake forecasts for 1999, *Seismol. Res.*
799 *Lett.*, **70**, 393-403.

800 Jackson, D. D., and Y. Y. Kagan (2012). 10 (abstract), Amer. Geophys. U. Fall Meeting 2012
801 abstract #S24A-08.

802 Kagan, Y. Y. (2003). Accuracy of modern global earthquake catalogs, *Phys. Earth Planet. Int.*,
803 **135**(2-3), 173-209, doi:10.1016/S0031-9201(02)00214-5.

804 Kagan, Y. Y. (2009). Testing long-term earthquake forecasts: Likelihood methods and error
805 diagrams, *Geophys. J. Int.*, **177**(2), 532-542.

806 Kagan, Y. Y., and D. D. Jackson (1991). Seismic gap hypothesis: Ten years after, *J. Geophys. Res.*,
807 **96**(B13), 21,419-21,431.

808 Kagan, Y. Y., and D. D. Jackson ([1994]). Long-term probabilistic forecasting of earthquakes, *J.*
809 *Geophys. Res.*, **99**, 13,685-13,700.

810 Kagan, Y. Y., and D. D. Jackson (2000). Probabilistic forecasting of earthquakes, *Geophys. J. Int.*,
811 **143**, 438-453.

812 Kagan, Y. Y. and D. D. Jackson (2011). Global earthquake forecasts, *Geophys. J. Int.*, **184**(2), 759-
813 776, doi: 10.1111/j.1365-246X.2010.04857.x

814 Kagan, Y. Y. and D. D. Jackson (2013). Tohoku earthquake: A surprise?, *Bull. Seismol. Soc. Am.*,
815 **103**(2B), 1181-1194.

816 Kagan, Y. Y., P. Bird, and D. D. Jackson (2010). Earthquake patterns in diverse tectonic zones of
817 the globe, *Pure Appl. Geoph.*, **167**(6/7), 721-741.

818 Kelleher, J., L. R. Sykes, and J. Oliver (1973). Possible criteria for predicting earthquake locations
819 and their application to major plate boundaries of the Pacific and the Caribbean, *J.*
820 *Geophys. Res.*, **78**, 2547-2585.

821 Kreemer, C., Blewitt, G., and Klein, E.C. (2014). A geodetic plate motion and Global Strain Rate
822 Model, *Geochem. Geophys. Geosyst.*, 15(10), 3849-3889, doi: 10.1002/2014GC005407.

823 Marzocchi, W., J. D. Zechar, and T. H. Jordan (2012). Bayesian forecast evaluation and ensemble
824 earthquake forecasting, *Bull. Seismol. Soc. Am.*, **102**(6), 2574-2584.

825 McCaffrey, R. (2008). Global frequency of magnitude 9 earthquakes, *Geology*, **36**(3), 263-266,
826 doi: 10.1120/G24402A.1.

827 McCann, W. R., S. P. Nishenko, L. R. Sykes, and J. Krause (1979). Seismic gaps and plate
828 tectonics: Seismic potential for major boundaries, *Pure Appl. Geoph.*, **117**, 1082-1147.

829 Michael, A. J. (2014). How complete is the ISC-GEM Global Earthquake Catalog?, *Bull. Seismol.*
830 *Soc. Am.*, **104**(4), 1829-1837.

831 Nishenko, S. P., and L. R. Sykes (1993). Comment on "Seismic gap hypothesis: Ten years after"
832 by Y. Y. Kagan and D. D. Jackson, *J. Geophys. Res.*, **98**(B6), 9909-9916.

833 Petersen, M. D., A. D. Frankel, S. C. Harmsen, C. S. Mueller, K. M. Haller, R. L. Wheeler, R. L.
834 Wesson, Y. Zeng, O. S. Boyd, D. M. Perkins, N. Luco, E. H. Field, C. J. Wills, and K. S.
835 Rukstales (2008). Documentation for the 2008 update of the United States National
836 Seismic Hazard Maps, *U.S. Geol. Surv. Open-File Rep.*, **2008-1128**, 128 pages.

837 Rhoades, D. A., and M. C. Gerstenberger (2009). Mixture models for improved short-term
838 earthquake forecasting, *Bull. Seismol. Soc. Am.*, **99**(2A), 636-646.

839 Rhoades, D. A., M. C. Gerstenberger, A. Christopherson, J. D. Zechar, D. Schorlemmer, M. J.
840 Werner, and T. H. Jordan (2013). Multiplicative hybrids of models from the five-year
841 RELM experiment (abstract), Southern California Earthquake Center, Annual Meeting
842 2013 Program, poster 265.

843 Rhoades, D. A., M. C. Gerstenberger, A. Christophersen, J. D. Zechar, D. Schorlemmer, M. J.
844 Werner, and T. H. Jordan (2014). Regional Earthquake Likelihood Models II: Information
845 Gains of Multiplicative Hybrids, *Bull. Seismol. Soc. Amer.*, **104**(1), doi:
846 10.1785/0120140035.

847 Schorlemmer, D., J. D. Zechar, M. J. Werner, E. H. Field, D. D. Jackson, T. H. Jordan, and the
848 RELM Working Group (2010). First results of the Regional Earthquake Likelihood Models
849 experiment, *Pure Appl. Geoph.*, **167**, 859-876, doi: 10.1007/s00024-010-0081-5.

850 Storchak, D. A., D. Di Giacomo, I. Bondar, J. Harris, E. R. Engdahl, W. H. K. Lee, A. Villasenor, P.
851 Bormann, and G. Ferrari (2012). ISC-GEM Global Instrumental Earthquake Catalog, 1900-
852 2009, *GEM Technical Report*, **2012-01**, 128 pages, doi: 10.13117/GEM.GEGD.TR2012.01,
853 Global Earthquake Model Foundation, Pavia, Italy.

854 Taroni, M., J. D. Zechar, and W. Marzocchi (2013). Assessing global M6+ seismicity forecasts,
855 *Geophys. J. Int.*, **136**, 422-432, doi: 10.1093/gji/ggt369.

856 Zechar, J. D. (2008). Methods for evaluating earthquake predictions, Ph.D. dissertation, U.
857 Southern California, Los Angeles.

858 Zechar, J. D., and T. H. Jordan (2008). Testing alarm-based earthquake predictions, *Geophys. J.*
859 *Int.*, **172**, 715-724, doi: 10.1111/j.1365-246X.2007.03676.x.

860 Zechar, J. D., M. C. Gerstenberger, and D. A. Rhoades (2010). Likelihood-based tests for
861 evaluation space-rate-magnitude earthquake forecasts, *Bull. Seismol. Soc. Am.*, **100**(3),
862 1184-1195, doi: 10.1785/0120090192.

863 AUTHORS

864 Peter Bird; Department of Earth, Planetary, and Space Sciences; University of California; Los
865 Angeles, CA 90095-1567.

866 David D. Jackson; Department of Earth, Planetary, and Space Sciences; University of California;
867 Los Angeles, CA 90095-1567.

868 Yan Y. Kagan; Department of Earth, Planetary, and Space Sciences; University of California; Los
869 Angeles, CA 90095-1567.

870 Corné Kreemer; Nevada Bureau of Mines and Geology; Seismological Laboratory; University of
871 Nevada; 1664 North Virginia Street; Reno, NV 89557-0178.

872 Ross S. Stein; U.S. Geological Survey; Office 3A113; 345 Middlefield Road, MS 977; Menlo Park,
873 CA 94025.

874 TABLE

875 **Table 1. Global shallow earthquake rates (*R*), per century:**

Catalog or model	<i>m</i>5.767+	<i>m</i>7+	<i>m</i>8+	<i>m</i>9+
ISC-GEM 1918-1976	N/A*	942	80	3
GCMT 1977-2013	17503	951	65	5
merged catalogs 1918-2013	N/A*	946	74	4
GEAR1, for 2014+	17589	1087	92	5
Seismicity, for 2014+	17647	1043	85	4
Tectonics, for 2014+	17503	1155	103	6

876 *N/A = Not Available (catalog incomplete).

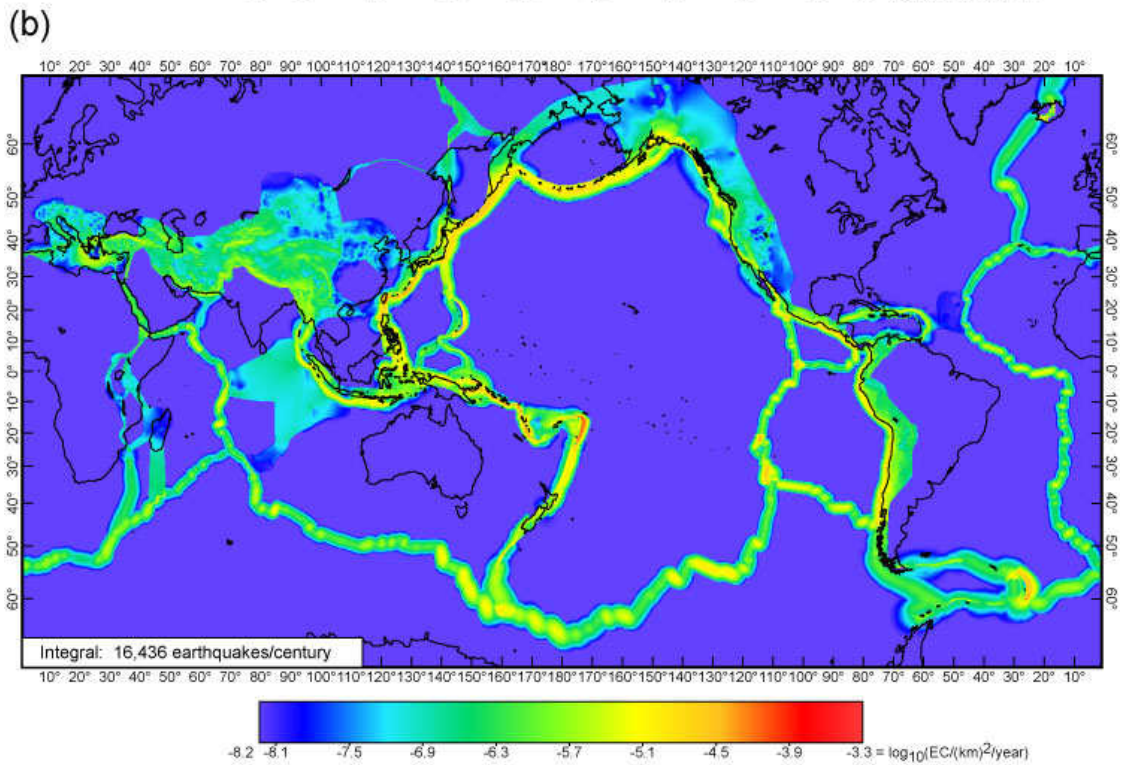
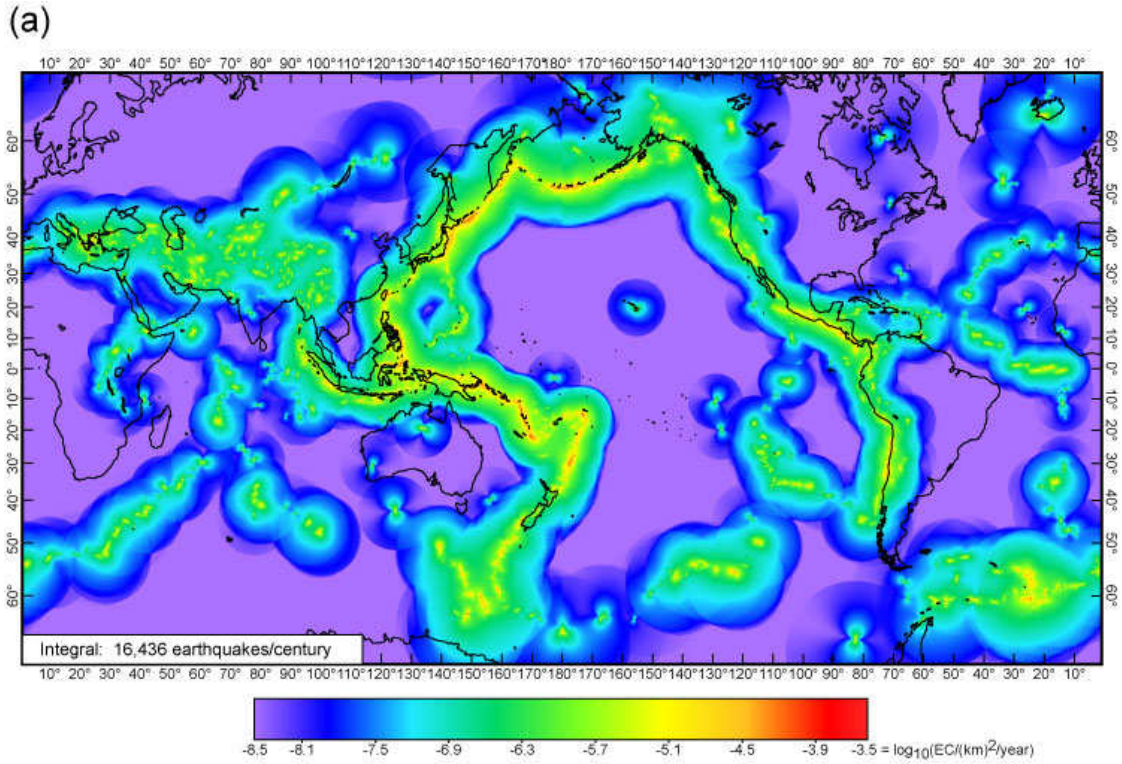
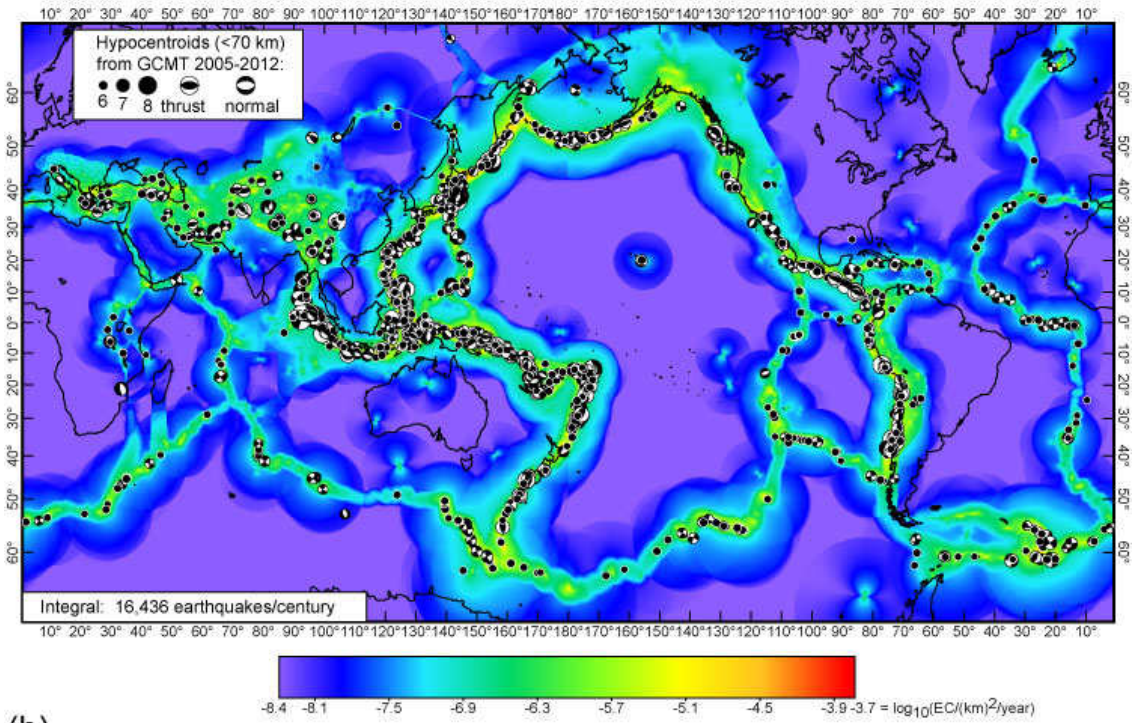


Figure 1. Two parent forecasts with threshold magnitude $m5.767+$: (a) Seismicity parent forecast for years 2005+. Mercator projection. Logarithmic color- (or gray-) scale shows the rate density of epicentroids corresponding to shallow (≤ 70 km) hypocentroids, in units of $(\text{km})^{-2} \text{ year}^{-1}$. (b) Tectonics parent forecast for years 2005+. Conventions as in part (A), and identical color- (or gray-) scale. Equal to model SHIFT-GSRM2f of Bird and Kreemer (2015), except that its original spatial grid of 0.25×0.20 -degree cells is here resampled to a finer 0.1×0.1 -degree grid. Colored maps appear in the online version.

878 .

(a)



(b)

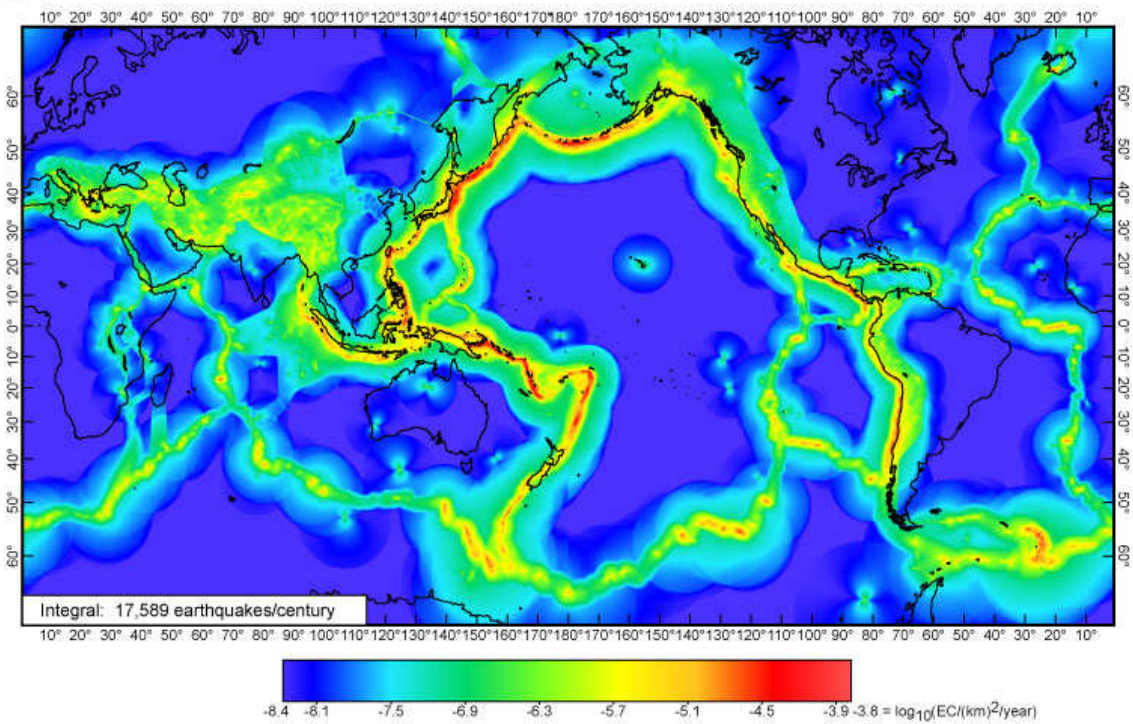


Figure 2. Preferred hybrid forecasts for threshold magnitude $m_{5.767+}$, both with and without overlay of test earthquakes: (a) Preferred hybrid forecast H^* (log-linear, with exponent $d = 0.6$ on Seismicity)

for years 2005+ compared to 1694 shallow test earthquakes from GCMT catalog years 2005-2012. For test earthquakes of $m > 6$, focal mechanism is shown on lower focal hemisphere. Scores from this comparison (and many others) are shown in Table S1 (available in the electronic supplement to this article) and Figure 3. (b) GEAR1 forecast (preferred hybrid H^* , updated to end-2013) for years 2014 and after. Mercator projection. Logarithmic color- (or gray-) scale shows the rate density of epicentroids corresponding to shallow (≤ 70 km) hypocentroids, in units of $(\text{km})^{-2} \text{ year}^{-1}$. Colored maps appear in the online version.

879 .

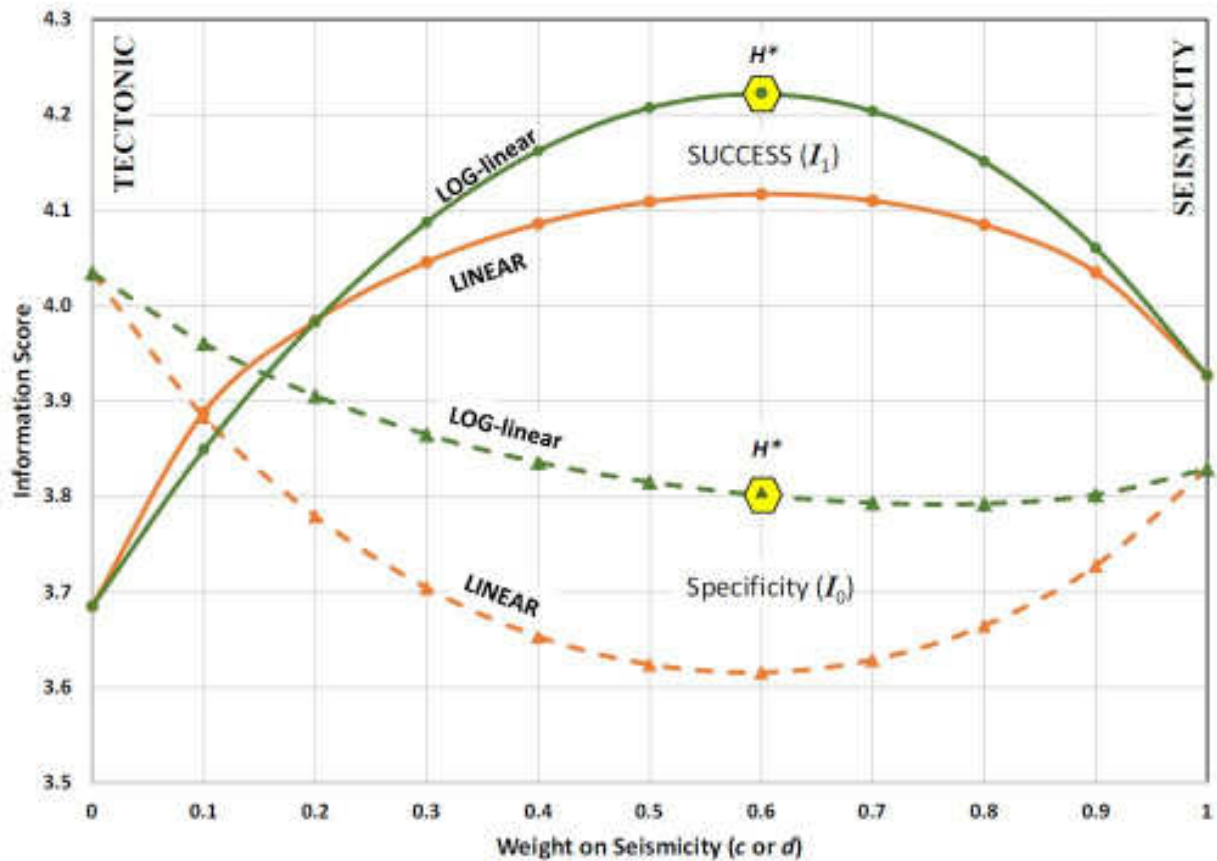


Figure 3. Success I_1 and specificity I_0 of both linear and log-linear hybrid models as a function of mixing parameter c or d , in tests against GCMT catalog years 2005-2012 at threshold $m_{5.767+}$. Both

of these I information scores were defined by Kagan [2009]. The preferred hybrid model H^* is highlighted.

880

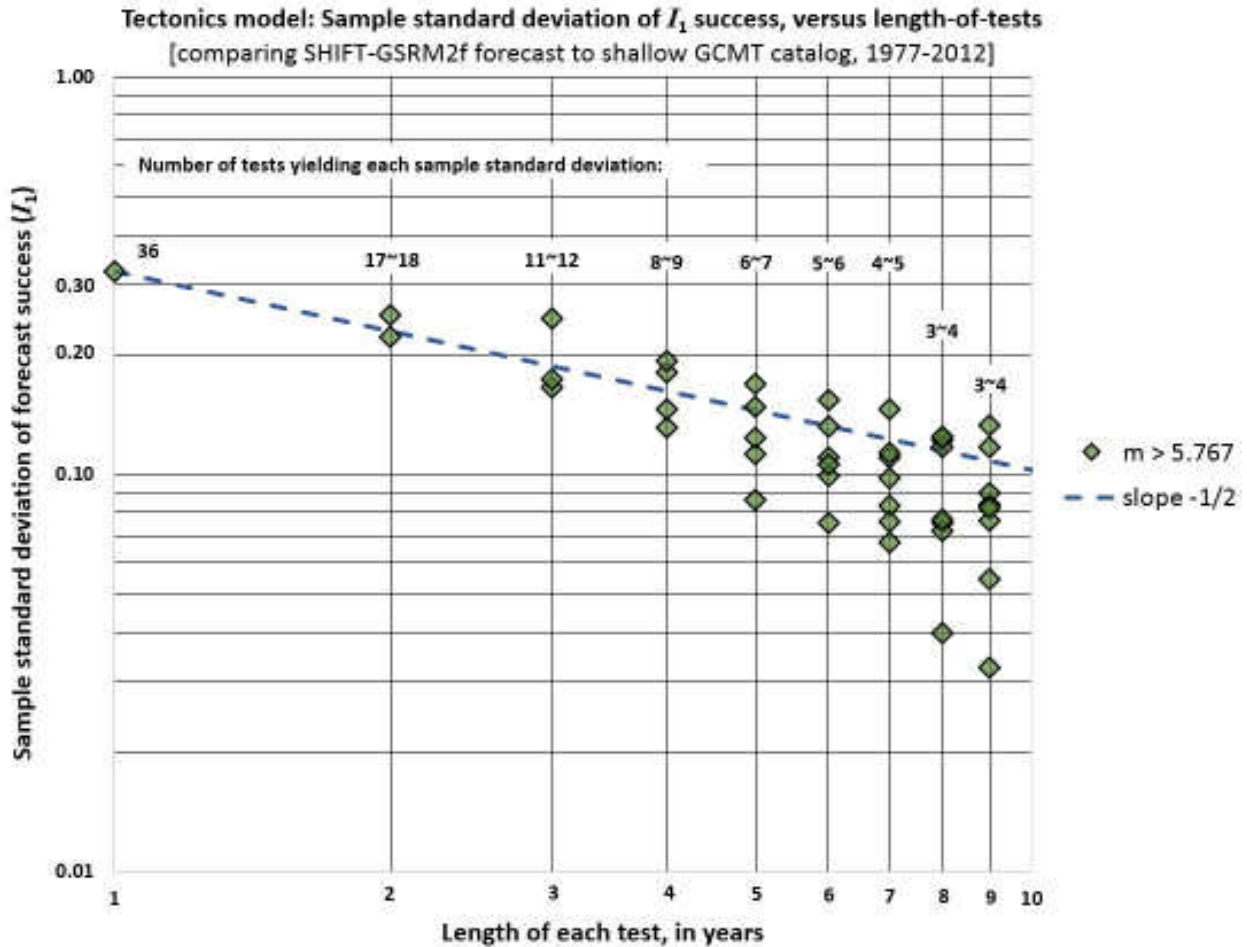


Figure 4. Small-sample standard deviations (diamonds) of the success of the Tectonics forecast, $\sigma(I_1(T))$, as a function of test window length W , in the range of 1 to 9 years. Based on multiple subdivisions (with re-use) of GCMT catalog years 1977-2012. Dashed line with slope -1/2 appears consistent with these bootstrap experimental results. There are 2 points at $W = 2$ years, 3 points at $W = 3$ years, etc., because these longer windows can be defined using W different start-years. The number of scores compared to compute each sample standard deviation decreases, with increasing W , from 36 to $3 \sim 4$, which explains

the increasing scatter of these sample standard deviations.

881 .

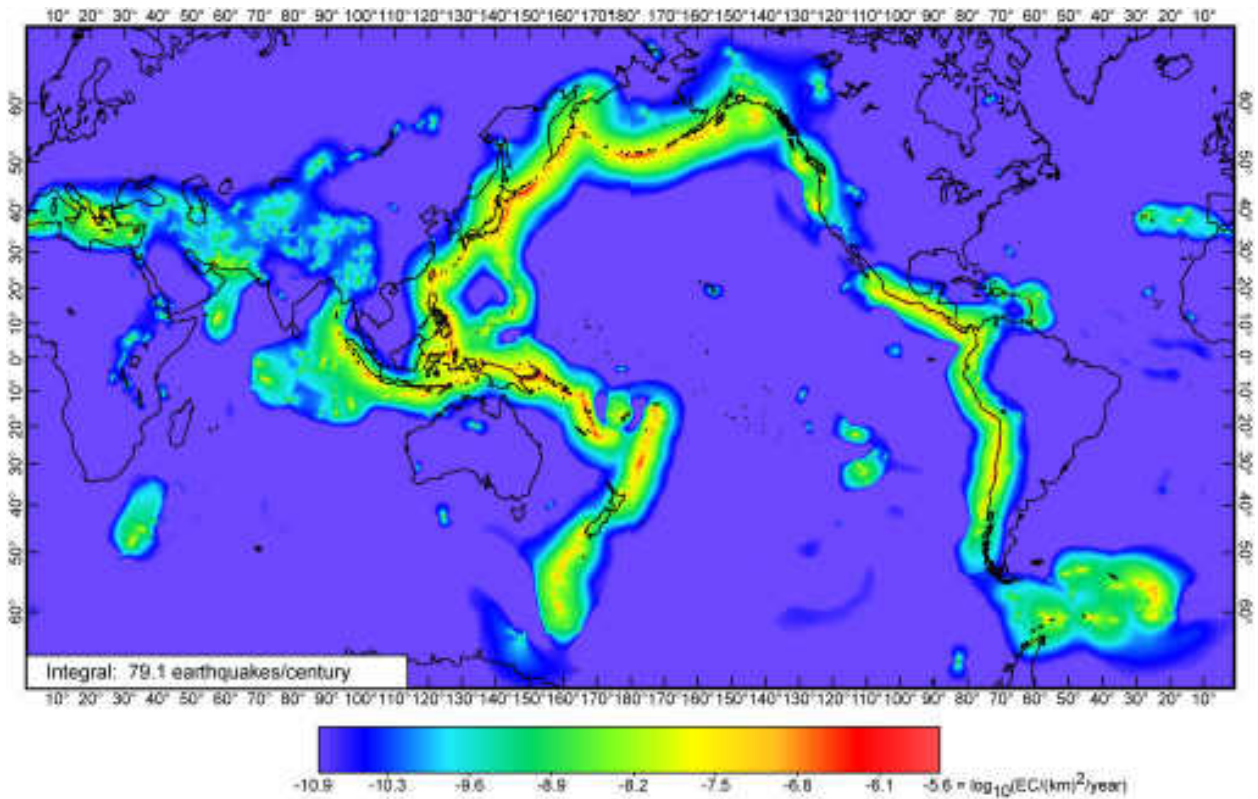


Figure 5. Extrapolation of the Seismicity parent forecast (from Figure 1A, for years 2005+) to threshold m_{8+} . Epicentroid rate density of each cell was extrapolated with the tapered Gutenberg-Richter frequency/magnitude distribution (8) using corner magnitudes and spectral slopes based on Table 1 of Kagan *et al.* (2010) and the tectonic zone map of the same paper, but only after edits and smoothing had been applied to the maps of corner magnitude and spectral slope, as described in text. Most spreading ridges have disappeared from this map because their corner magnitudes are less than the m_{8+} threshold. A few active spots remain where oceanic transform slip is transpressive; because slip-partitioning into thrust earthquakes is expected, these regions were assigned to tectonic zone 4 by Kagan *et al.* (2010). Colored map appears in the online version.

882 .

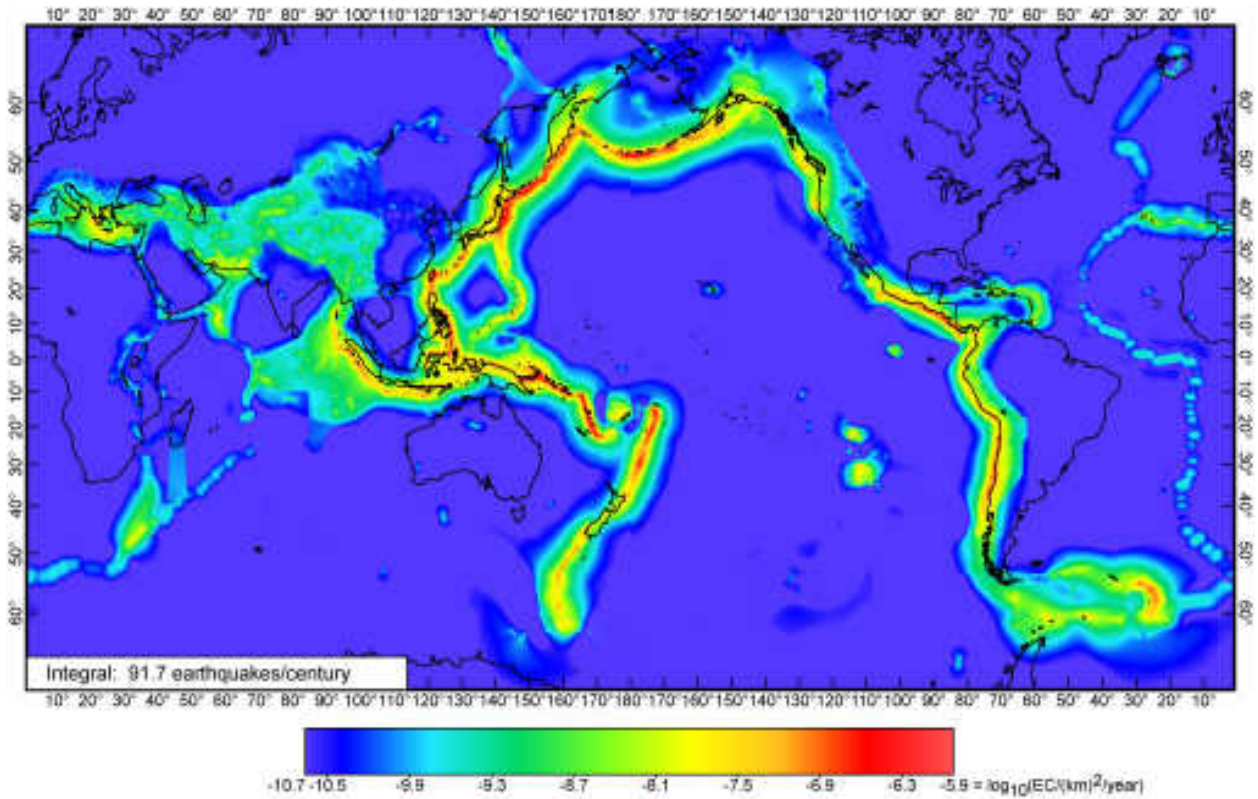


Figure 6. GEAR1 forecast for threshold magnitude $m8+$ and for years 2014 and after. Conventions as in Figure 2B. Global earthquake rate is based on (9). This map has strong similarities to the parent Seismicity forecast of Figure 5, but also reflects the influence of the Tectonics parent forecast in its better depiction and resolution of plate boundary zones, and also the updating of both parent forecasts to the end of 2013. Colored map appears in the online version.

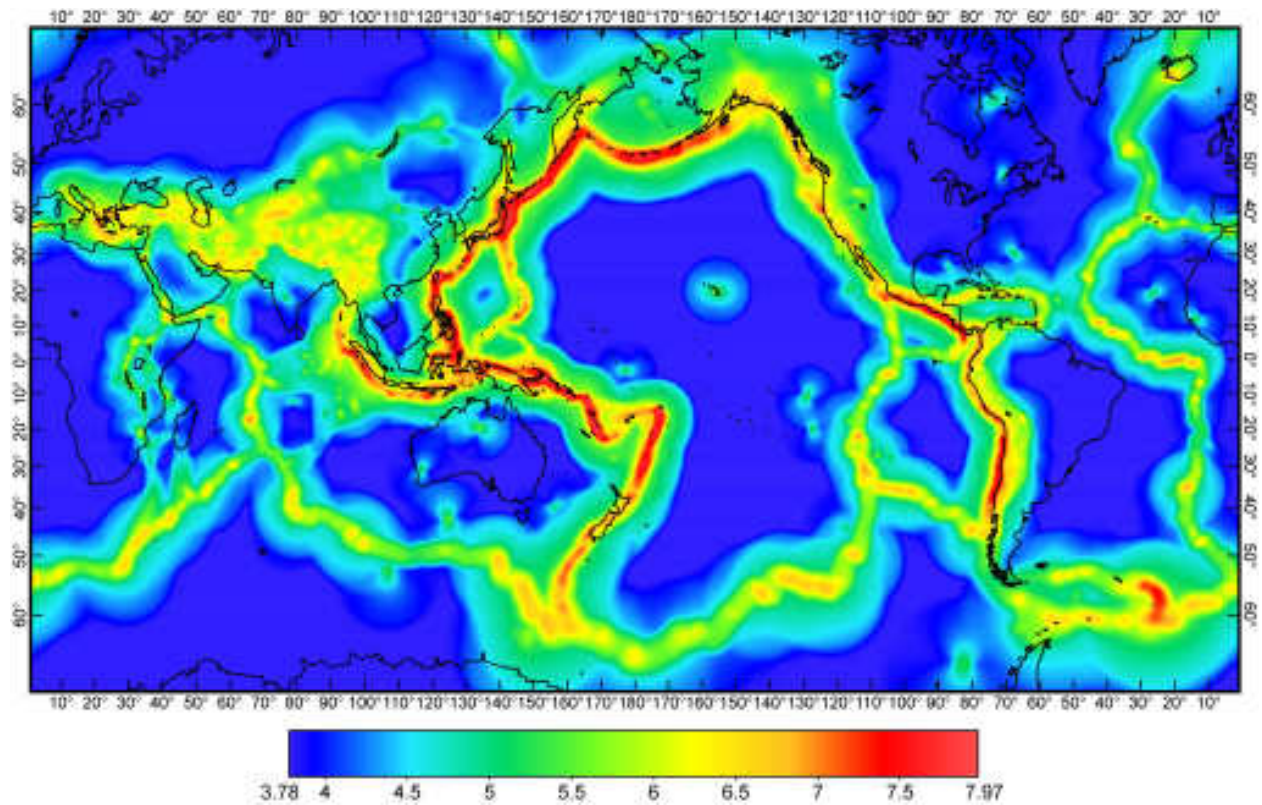


Figure 7. GEAR1 forecast for years 2014 and after, represented as the magnitude that has forecast epicentroid rate of 0.01/year (*i.e.*, probability of approximately 1% per year) within a local circle of radius 100 km about each test point. Colored map appears in the online version.

884 .

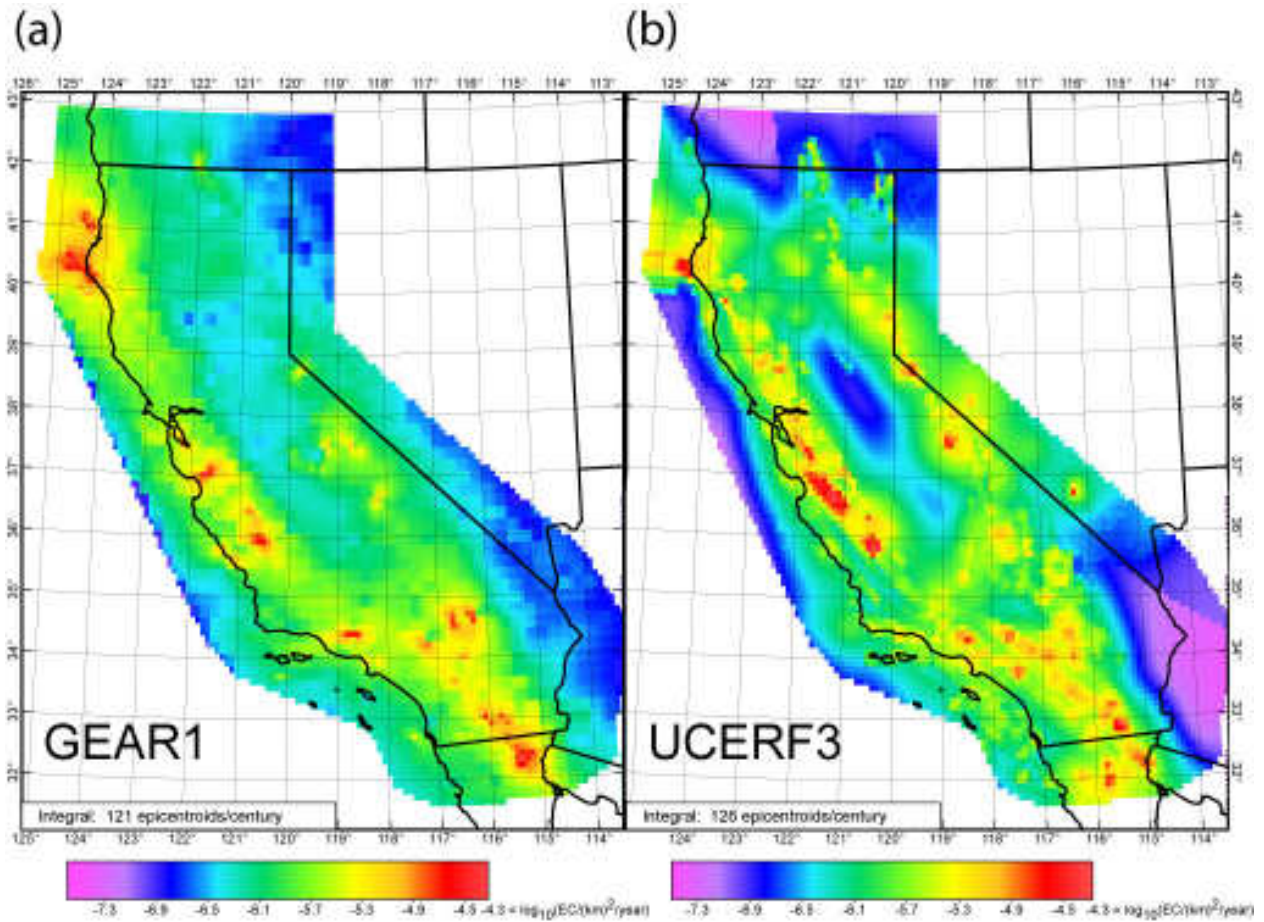


Figure 8. Comparison of: (a) GEAR1 long-term epicentroid rate densities in the California region at threshold magnitude $m5.8+$, with: (b) the branch-weighted mean time-independent seismicity forecast UCERF3 by Field *et al.* (2013) at the same threshold. The GEAR1 forecast has been windowed to match the area covered by UCERF3. Note that the UCERF3 forecast has not been smoothed for this figure, although smoothing is discussed in the text. Statistics of the comparison are presented in the text. Colored maps appear in the online version.

1 Electronic Supplement to:

2 GEAR1: a Global Earthquake Activity Rate model constructed from
3 geodetic strain rates and smoothed seismicity

4 P. Bird, D. D. Jackson, Y. Y. Kagan, C. Kreemer, and R. S. Stein

5 These Electronic Supplement files include additional text and references on scoring of forecasts,
6 tables of scoring results, and source code and data files needed to reproduce our forecast.

7
8 **Table Captions:**

9 Table S1: Results of 8-year retrospective tests against shallow events from GCMT, 2005-2012;

10 Table S2: One-year I_1 success scores against shallow events in GCMT, 2005-2012;

11 Table S3: Results of 59-year retrospective tests against shallow ISC-GEM, 1918-1976;

12
13 **Other:**

14 *Fortran 90 source code in file GEAR1_for_CSEP.f90 (for computing GEAR1);

15 *GEAR1_parameters.dat (primary input file for computing GEAR1);

16 *Smoothed-seismicity parent forecast in file GL_HAZTBLT_M5_B2_2013.TMP.zip (56 MB
17 compressed version of 349 MB ASCII file GL_HAZTBLT_M5_B2_2013.TMP).

18
19
20 Discussion of forecast-scoring metrics

21 Some seismic forecast test metrics consider only the number of earthquakes; some consider
22 only the map-pattern; others consider both. When testing forecast numbers of earthquakes, it
23 is critical to take into account earthquake clustering on all scales, which causes annual
24 earthquake counts to have a distribution much broader than a Poisson distribution, which is
25 probably best described by the negative-binomial distribution (Kagan, 2010). Such a revised
26 number-test would be a valuable tool for testing forecasts of total seismicity. However, to date
27 no such test is a recognized standard (*e.g.*, operational at the Collaboratory for the Study of

28 Earthquake Predictability, or CSEP). Instead, CSEP employs the N-test (Field, 2007;
29 Schorlemmer and Gerstenberger, 2007; Schorlemmer *et al.*, 2007, 2010; Zechar *et al.*, 2010)
30 which assumes that test earthquakes are mutually independent. This assumption of
31 independence requires both the forecast and the test catalog to be declustered prior to testing.
32 Unfortunately, there is no obvious method available for declustering our two parent forecasts
33 or our hybrid forecasts, so we cannot use such tests. We also decline to emulate the L-test and
34 R-test of CSEP (*ibid*), which have similar issues requiring declustering. Here, we will consider
35 test metrics that compare only the map-patterns of forecast and test seismicity, independent of
36 earthquake counts.

37 Our preferred measures of forecast specificity and success are two of the information scores (I)
38 defined by Kagan (2009). “Success” measure I_1 is the mean, over all test earthquakes, of the
39 base-2 logarithm of the ratio of conditional probability density in the cell in which the test
40 earthquake epicentroid occurred, to the mean conditional probability density in the whole
41 forecast region (which, in this paper, is the shallow part of the Earth). Here, “conditional
42 probability” is the probability of an earthquake appearing with epicentroid at a particular
43 (longitude, latitude) point, conditional on the occurrence of one new earthquake somewhere in
44 the forecast domain with magnitude at or above threshold. Thus, I_1 is the mean number of
45 binary bits of information gain per actual test earthquake, over an ignorant model that has only
46 a single global earthquake rate. “Specificity” I_0 is the sum over all forecast cells of the
47 normalized forecast rate times the base-2 logarithm of the ratio of normalized forecast rate to
48 normalized cell area. Thus, I_0 is the mean number of binary bits of information gain (per
49 virtual, expected earthquake), over an ignorant model that has only a single global earthquake

50 rate. Note that specificity I_0 does not require or use the test catalog, so it is an interesting
51 descriptor of the forecast, but less important than success I_1 . These information scores have
52 several advantages: scores are independent of any difference between the total numbers of
53 forecast and test earthquakes; no simulated virtual catalogs based on the forecast are needed;
54 no random perturbations of the test catalog are needed; declustering is not used; the success
55 has a normal distribution across repeated tests when the number of test earthquakes is large
56 (Kagan, 2009); and the results are on an absolute scale. The rate-corrected average-
57 information-gain tests (T- and W-tests) of Rhoades *et al.* (2011) are similar but not identical.
58 As another measure of forecast map-patterns, we use the space statistic “S” (Zechar *et al.*,
59 2010) which is a variant of the L-test implemented at CSEP, but with the dependence on
60 earthquake count removed. Specifically, we scale each forecast under test to the actual rate of
61 earthquakes during the test period, to eliminate any direct earthquake-count factors in the
62 likelihoods. As in the implementation of the L-test used at CSEP we simulate a number (1000)
63 of virtual test catalogs from the forecast to experimentally describe the sample-size effect on
64 test precision. No clustering or aftershock sequences are simulated in these virtual catalogs.
65 The S-statistic is the fraction of simulations in which the (single) test-catalog “log-likelihood”
66 exceeds the virtual-catalog “log-likelihood.” If this statistic is less than 0.05, some consider the
67 forecast should be rejected. However, note that (unlike CSEP) we have not declustered either
68 the forecast or the test catalog. Consequently, our “log-likelihoods” are only biased estimates
69 of true log-likelihoods, and our S-statistic is not really a probability, so applying any hard cutoff
70 is inappropriate. Still, models that give a very low value of the S statistic are likely to have
71 lower quality. Interestingly, a very high value of the S statistic (> 0.5) can be a sign of potential

72 for improvement; it shows that test earthquakes consistently fell in the areas of maximum
73 forecast probability, but that the intermediate-probability “shoulders” of the forecast were
74 lightly populated with fewer than predicted test earthquakes, and may be broader than
75 necessary.

76 References cited

- 77 Field, E. H. (2007). Overview of the Working Group for the Development of Regional Earthquake
78 Likelihood Models (RELM), in: S. E. Hough and K. B. Olsen (ed.), Special Issue on:
79 Regional Earthquake Likelihood Models, *Seismol. Res. Lett.*, **78**(1), 7-16.
- 80 Kagan, Y. Y. (2009). Testing long-term earthquake forecasts: Likelihood methods and error
81 diagrams, *Geophys. J. Int.*, **177**(2), 532-542.
- 82 Kagan, Y. Y. (2010). Statistical distributions of earthquake numbers: Consequences of branching
83 process, *Geophys. J. Int.*, **80**(3), 1313-1328, doi: 10.1111/j.1365-246X.2009.04487.x.
- 84 Rhoades, D. A., D. Schorlemmer, M. C. Gerstenberger, A. Christopherson, J. D. Zechar, and M.
85 Imoto (2011). Efficient testing of earthquake forecasting models, *Acta Geophys.*, **59**,
86 728-747.
- 87 Schorlemmer, D., and M. Gerstenberger (2007). RELM Testing Center, *Seismol. Res. Lett.*, **78**(1),
88 30-36.
- 89 Schorlemmer, D., M. C. Gerstenberger, W. Wiemer, D. D. Jackson, and D. A. Rhoades (2007).
90 Earthquake likelihood model testing, in: S. E. Hough and K. B. Olsen (ed.), Special Issue
91 on: Regional Earthquake Likelihood Models, *Seismol. Res. Lett.*, **78**(1), 17-29.

92 Schorlemmer, D., J. D. Zechar, M. J. Werner, E. H. Field, D. D. Jackson, T. H. Jordan, and the
93 RELM Working Group (2010). First results of the Regional Earthquake Likelihood Models
94 experiment, *Pure Appl. Geoph.*, **167**, 859-876, doi: 10.1007/s00024-010-0081-5.
95 Zechar, J. D., M. C. Gerstenberger, and D. A. Rhoades (2010). Likelihood-based tests for
96 evaluating space-rate-magnitude earthquake forecasts, *Bull. Seismol. Soc. Am.*, **100**(3),
97 1184-1195, doi: 10.1785/0120090192.

Table S1. Results of 8-year retrospective tests against shallow events from GCMT, 2005-2012:

Threshold:	<i>m</i> 5.767+ (<i>N</i> = 1694)			<i>m</i> 7+ (<i>N</i> = 90)		
Model Class, <i>c</i> or <i>d</i>	Speci- ficity (<i>I</i> ₀)	Success (<i>I</i> ₁)	S statis- tic	Speci- ficity (<i>I</i> ₀)	Success (<i>I</i> ₁)	S statis- tic
Envelope	3.607	4.00	0.960	3.745	4.0	0.61
Tectonic (<i>c</i> = 0)	4.034	3.69	0.023	4.347	3.8	0.35
Linear, <i>c</i> = 0.1	3.884	3.89	0.426	4.154	4.0	0.46
Linear, <i>c</i> = 0.2	3.779	3.98	0.806	4.012	4.1	0.54
Linear, <i>c</i> = 0.3	3.704	4.05	0.932	3.903	4.1	0.56
Linear, <i>c</i> = 0.4	3.653	4.09	0.971	3.819	4.1	0.56
Linear, <i>c</i> = 0.5	3.624	4.11	0.983	3.758	4.1	0.62
Linear, <i>c</i> = 0.6	3.616	4.12	0.986	3.720	4.1	0.62
Linear, <i>c</i> = 0.7	3.629	4.11	0.977	3.704	4.1	0.63
Linear, <i>c</i> = 0.8	3.665	4.08	0.969	3.713	4.0	0.59
Linear, <i>c</i> = 0.9	3.728	4.03	0.884	3.750	3.9	0.57
Seismicity (<i>c</i> =1)	3.829	3.93	0.584	3.829	3.8	0.48
Tectonic (<i>d</i> = 0)	4.034	3.69	0.023	4.347	3.8	0.35
Log-linear, <i>d</i> =0.1	3.960	3.85	0.234	4.232	4.0	0.43
Log-linear,	3.906	3.98	0.572	4.143	4.1	0.52

$d=0.2$						
Log-linear, $d=0.3$	3.865	4.09	0.827	4.072	4.2	0.55
Log-linear, $d=0.4$	3.836	4.16	0.927	4.013	4.2	0.54
Log-linear, $d=0.5$	3.815	4.21	0.968	3.962	4.2	0.58
Log-linear, $d=0.6$ (H*)	3.801	4.22	0.971	3.917	4.2	0.59
Log-linear, $d=0.7$	3.793	4.20	0.962	3.877	4.2	0.59
Log-linear, $d=0.8$	3.792	4.15	0.931	3.843	4.1	0.58
Log-linear, $d=0.9$	3.802	4.06	0.833	3.823	3.9	0.54
Seismicity ($d=1$)	3.829	3.93	0.584	3.829	3.8	0.48

m : magnitude; N : number of test earthquakes; c , d : mixing coefficients of hybrid forecasts,

defined in main text; I_0 , I_1 : forecast scores of Kagan (2009); S-statistic defined by Zechar *et al.*

(2010).

Table S2. One-year I_1 success scores against shallow events in GCMT, 2005-2012:

Threshold:	$m5.767+$ ($N \cong 212/\text{year}$)			$m7+$ ($N \cong 11/\text{year}$)		
Year	$I_1(H^*)$	$I_1(S)$	$I_1(H^*)-I_1(S)$	$I_1(H^*)$	$I_1(S)$	$I_1(H^*)-I_1(S)$
2005	3.8843	3.7445	0.1398	3.3317	2.4809	0.8508
2006	3.9901	3.5784	0.4117	3.1494	2.3293	0.8201
2007	4.2486	3.9903	0.2583	4.9593	4.5226	0.4367
2008	3.9290	3.6740	0.2550	3.5888	3.6086	-0.0198
2009	4.3836	4.0526	0.3310	4.7456	4.5973	0.1483
2010	4.2299	3.8480	0.3819	4.2105	3.4980	0.7125
2011	4.8201	4.4914	0.3287	4.6979	4.3939	0.3040
2012	4.1738	3.9273	0.2465	3.9932	3.4583	0.5349
Mean:	4.2074	3.9133	0.2941	4.0846	3.6111	0.4734
Standard Deviation:	0.3021	0.2833	0.0870	0.6855	0.8761	0.3168
Correlation:	0.9578			0.9467		

m : magnitude; N : number of test earthquakes; I_1 : forecast score of Kagan (2009); H^* : preferred hybrid forecast; S : Seismicity parent forecast.

Table S3. Results of 59-year retrospective tests against shallow events from ISC-GEM, 1918-1976:

	<i>m</i> 6.8+ (<i>N</i> = 881)		
Model Class, <i>c</i> or <i>d</i>	Speci- ficity (<i>I</i>₀)	Success (<i>I</i>₁)	S statis- tic
Envelope	3.729	3.60	0.305
Tectonic (<i>c</i> = 0)	4.292	3.41	0.000
Linear, <i>c</i> = 0.1	4.108	3.59	0.034
Linear, <i>c</i> = 0.2	3.975	3.66	0.130
Linear, <i>c</i> = 0.3	3.872	3.70	0.289
Linear, <i>c</i> = 0.4	3.794	3.72	0.351
Linear, <i>c</i> = 0.5	3.738	3.72	0.455
Linear, <i>c</i> = 0.6	3.705	3.71	0.458
Linear, <i>c</i> = 0.7	3.694	3.69	0.429
Linear, <i>c</i> = 0.8	3.706	3.64	0.402
Linear, <i>c</i> = 0.9	3.747	3.56	0.237
Seismicity (<i>c</i> = 1)	3.829	3.39	0.073
Tectonic (<i>d</i> = 0)	4.292	3.41	0.000
Log-linear, <i>d</i> = 0.1	4.180	3.56	0.016
Log-linear, <i>d</i> = 0.2	4.092	3.67	0.065
Log-linear, <i>d</i> = 0.3	4.023	3.75	0.178

Log-linear, $d = 0.4$	3.967	3.80	0.253
Log-linear, $d = 0.5$	3.921	3.82	0.327
Log-linear, $d = 0.6$	3.883	3.81	0.359
Log-linear, $d = 0.7$	3.851	3.76	0.344
Log-linear, $d = 0.8$	3.828	3.68	0.274
Log-linear, $d = 0.9$	3.817	3.55	0.166
Seismicity ($d = 1$)	3.829	3.39	0.073

m : magnitude; N : number of test earthquakes; c , d : mixing coefficients of hybrid forecasts, defined in main text; I_0 , I_1 : forecast scores of Kagan (2009); S-statistic defined by Zechar *et al.* (2010).